Plasmodium falciparum **MORC protein modulates gene expression through interaction with heterochromatin**

Maneesh Kumar Singh[1#], Victoria A. Bonnell[2,3,4#], Israel Tojal Da Silva[5], Verônica Feijoli Santiago[6], Miriam S. Moraes[1], Jack Adderley[7], Christian Doerig[7], Giuseppe Palmisano[6], Manuel Llinás[2,3,4,8], and Célia R. S. Garcia[1]*

[1] Department of Clinical and Toxicological Analyses, School of Pharmaceutical Sciences, University of São Paulo, São Paulo, Brazil

[2] Department of Biochemistry and Molecular Biology, Pennsylvania State University, University Park, Pennsylvania, United States

[3] Huck Institutes Center for Eukaryotic Gene Regulation, Pennsylvania State University, University Park, Pennsylvania, United States

[4] Huck Institutes Center for Malaria Research, Pennsylvania State University, University Park, Pennsylvania, United States

[5] Hospital AC Camargo, Centro Internacional de Pesquisa, São Paulo, Brazil

[6] Department of Parasitology, Institute of Biomedical Science, University of São Paulo, São Paulo, Brazil

[7] School of Health and Biomedical Sciences, RMIT University, Bundoora, Melbourne, VIC 3083, Australia

[8] Department of Chemistry, Pennsylvania State University, University Park, Pennsylvania, United States

 # coauthorship

*** Corresponding author**

Abstract

Dynamic control of gene expression is critical for blood stage development of malaria parasites. Here, we used multi-omic analyses to investigate transcriptional regulation by the chromatin-associated microrchidia protein, MORC, during asexual blood stage development of the human malaria parasite *Plasmodium falciparum*. *Pf*MORC (PF3D7_1468100) interacts with a suite of nuclear proteins, including APETALA2 (AP2) transcription factors (*Pf*AP2-G5, *Pf*AP2-O5, *Pf*AP2-I, PF3D7_0420300, PF3D7_0613800, PF3D7_1107800, and PF3D7_1239200), a DNA helicase DS60 (PF3D7_1227100), and other chromatin remodelers (*Pf*CHD1, *Pf*EELM2, and *Pf*ISWI). Transcriptomic analysis of *Pf*MORC$^{\text{HA-glmS}}$ knockdown parasites revealed 163 differentially expressed genes belonging to hypervariable multigene families, along with upregulation of genes mostly involved in host cell invasion. *In vivo* genome-wide chromatin occupancy analysis during both trophozoite and schizont stages of development demonstrates that *Pf*MORC is recruited to repressed, multigene families, including the *var* genes in subtelomeric chromosomal regions. Collectively, we find that *Pf*MORC is found in chromatin complexes that play a role in the epigenetic control of asexual blood stage transcriptional regulation.

Introduction

Despite global efforts to combat malaria, the disease caused an estimated 247 million new cases and more than 619,000 deaths in 2021 (World Malaria Report 2022). The etiological agents of human malaria are apicomplexan parasites of the genus *Plasmodium*. Among the six known *Plasmodium* species that can infect humans, *Plasmodium falciparum* is the most lethal, causing the majority of annual deaths if left untreated (Cowman et al. 2012). The intraerythrocytic developmental cycle (IDC) of *P. falciparum* is responsible for the clinical symptoms of malaria. The IDC commences when liver-stage merozoites enter the circulatory system and invade red blood cells (RBCs). While growing inside RBCs, parasites undergo multiple developmental phases with distinct morphological characteristics (ring, trophozoite, and schizont). Maturation and schizogony leads to the formation of 16-32 daughter merozoites destined to invade new RBCs (Singh et al. 2010). A small fraction (<10%) of parasites differentiate into non-replicative sexual gametocytes, which are transmitted to the mosquito during a second blood meal to complete sexual development.

Parasite development through the asexual blood stage is facilitated by precise transcriptional regulation, where genes are only expressed when needed in a just-in-time fashion (Bozdech et al. 2003). Approximately 90% of genes across the *P. falciparum* genome are transcribed during the asexual blood stage in a cascade of gene expression believed to be controlled by both sequence-specific transcription factors and dynamic epigenetic changes to chromatin (Painter et al. 2011, Toenhake et al. 2018, Jeninga et al. 2019, Hollin et al. 2021). The typical gene regulatory toolbox in malaria parasites is lacking many transcriptional regulatory factors conserved in other eukaryotes (Gardner et al. 2002). The identification of *Plasmodium* homologues of the plant APETALA2/Ethylene Response Factor (AP2/ERF) transcription factors (TFs) provided a breakthrough to unravel key regulators of gene expression in these parasites (Balaji et al. 2005). There are 28 putative APETALA2 (ApiAP2) TFs identified in *P. falciparum,* each protein containing one to three AP2 DNA binding domains (Painter et al. 2011, Jeninga et al. 2019). Multiple studies in *Plasmodium spp.,* using a variety of approaches, have characterized essential functions of ApiAP2 TFs in RBC invasion, gametocytogenesis, oocyst formation and sporozoite formation (Yuda et al. 2009, Kafsack et al. 2014, Sinha et al. 2014, Modrzynska et al. 2017, Santos et al. 2017, Zhang et al. 2018). ApiAP2 proteins in *Plasmodium* species display a wide array of functions during parasite development in both the vertebrate host and the mosquito vector, but surprisingly, approximately 70% of ApiAP2 proteins are expressed in the asexual blood stage of the lifecycle (Bozdech et al. 2003, Le Roch et al. 2003).

Despite increasing evidence detailing ApiAP2 protein regulatory complexes (Santos et al. 2017, Harris et al. 2019, Hillier et al. 2019, Hoeijmakers et al. 2019, Farhat et al. 2020, Josling et al. 2020, Miao et al. 2021, Antunes et al. 2023, Srivastava et al. 2023, Yuda et al. 2023), the functional properties and specific interaction partners of many ApiAP2 TFs remain to be elucidated. A quantitative mass spectrometry-based analysis of the parasite protein interaction network has revealed links between ApiAP2 TFs and many chromatin remodelers, such as an extended Egl-27 and MTA1 homology 2 (EELM2) domain-containing proteins (PF3D7_0519800 and PF3D7_1141800), histone deacetylase protein 1 (HDAC1; PF3D7_0925700), and the microrchidia family protein *Pf*MORC (PF3D7_1468100) (Hillier et al. 2019). Genome-wide mutagenesis studies revealed that several genes within these proposed networks, including *pfmorc*, are essential for parasite proliferation (Bushell et al. 2017, Zhang et al. 2018). Using a targeted deletion strategy, we previously were unable to delete *pfmorc,* further suggesting that it is essential for parasite growth (Singh et al. 2021). Moreover, STRING network analysis has shown that the putative ApiAP2:*Pf*MORC complex forms a network with proteins having DNA-binding or nucleosome assembly properties, suggesting that *Pf*MORC may function as an accessory protein in epigenetic regulation (Hillier et al. 2019). Previous work identified *Pf*MORC in a chromatin complex containing the chromatin remodeling protein *Pf*ISWI (PF3D7_0624600) located at *var* gene promoter regions (Bryant et al. 2020). Bryant et al. proposed that *Pf*MORC is recruited to these regions to help repress silenced *var* genes on the basis of its known function as a repressor complex component in model eukaryotes. In the related apicomplexan parasite *Toxoplasma gondii*, *Tg*MORC functions as a repressor of sex-associated genes by recruiting the histone deacetylase protein *Tg*HDAC3 and forming heterogenous complexes with eleven ApiAP2 TFs (Farhat et al. 2020). To date, only two *Tg*MORC:HDAC3 complexes have been characterized, including a *Tg*AP2XII-2:HDAC3 complex and a heterotrimeric *Tg*AP2XII-1:AP2XI-2:HDAC3 complex (Antunes et al. 2023, Srivastava et al. 2023).

MORC proteins canonically consist of two major conserved regions: (1) a catalytic ATPase domain at the N-terminus (contains a GHKL [Gyrase, HSP90, Histidine kinase, and MutL] domain and S5 fold domain) and (2) a C-terminal protein-protein interaction domain with one or more coiled-coils (Koch et al. 2017). The MORC family of proteins is highly conserved in all eukaryotic cells, with the exception of fungi, often with multiple paralogs per genome (Dong et al. 2018), and has been extensively investigated in model various systems in the context of epigenetic gene regulation. For example, in plants MORC family proteins function in gene repression and heterochromatin compaction (Koch et al. 2017, Zhong et al. 2023). Additionally,

107 MORC family proteins have been shown to play diverse roles by forming protein-protein
108 interactions with immune-responsive proteins, SWI chromatin remodeling complexes, histone
109 deacetylases, and histone tail modifications across metazoans (Iyer et al. 2008, Kang et al. 2012,
110 Moissiard et al. 2012, Bordiya et al. 2016, Kim et al. 2019).
111 While most metazoans possess five to seven MORC paralogs, apicomplexan parasites contain
112 a single *morc* gene (Iyer et al. 2008), which encodes not only the canonical animal-like GHKL
113 ATPase domain, but also three Kelch-repeats, and a CW-type zinc-finger domain not found in
114 mammalian MORCs (Farhat et al. 2020). This unique domain architecture suggests that the
115 Apicomplexan MORC proteins may have parasite-specific roles. To dissect the functional roles
116 of *Pf*MORC, we conducted a proteomic analysis with *Pf*MORC^{GFP} which identified several
117 nuclear proteins, including a cluster of ApiAP2 TFs, as possible interacting partners. We also
118 determined the genome-wide localization of *Pf*MORC at multiple developmental stages, which
119 revealed *Pf*MORC recruitment predominantly to subtelomeric regions, corroborating that
120 *Pf*MORC may act as a repressor of clonally variant gene families. Finally, we performed
121 transcriptomic analysis in *Pf*MORC$^{HA\text{-}glmS}$ knockdown parasites at the asexual stage to
122 investigate alterations in global gene expression. Our results indicate an overrepresentation of
123 downregulated genes belonging to the heterochromatin-associated hypervariable gene family
124 proteins. Overall, this study allows us to understand the plasticity in epigenetic regulation via
125 *Pf*MORC during asexual blood stage development.
126

127 # Results

128 ***Enriched proteins represent gene regulatory and chromatin remodeling components***

129 A previous study using Blue-Native PAGE identified a *Pf*MORC complex in association with
130 other ApiAP2 proteins and chromatin remodeling machinery (Hillier et al. 2019). To validate the
131 interacting partners of *Pf*MORC, we used a targeted immunoprecipitation approach coupled to
132 LC–MS/MS proteomic quantification. We used a previously generated *Pf*MORC^{GFP} parasite line
133 (Singh et al. 2021) to carry out immunoprecipitation with an anti-GFP antibody at the trophozoite
134 stage, where *Pf*MORC is abundant (Singh *et al*. 2021). The *P. falciparum* 3D7 strain expressing
135 wild-type *pfmorc* was used as a negative control. Trophozoite lysates were incubated with anti-
136 GFP-Trap-A beads (ChromoTek, gta-20), and the immunocaptured proteins were resolved by
137 SDS–PAGE (**Supplemental Figure 1A**). We applied a label-free quantitative proteomics
138 approach with a false discovery rate (FDR) of 1% and number of peptides ≥2 to excised gel
139 samples to identify proteins interacting with *Pf*MORC^{GFP}. From three replicates, we identified

140 211, 617, and 656 proteins respectively (**Figure 1B, Supplemental Table 1**). We further
141 identified the overlap between all three wild-type 3D7 and PfMORC^{GFP} replicates and found a
142 total of 132 and 142 proteins, respectively (**Supplemental Figure 1C**).
143 To analyze the relative ratio of proteins between wild-type 3D7 and *Pf*MORC^{GFP} groups, we used
144 the mean normalized MS/MS count to calculate a fold change and selected differentially abundant
145 proteins above a 1.5x cutoff filter. This resulted in 143 significantly enriched proteins
146 (**Supplemental Table 2**). From these candidate PfMORC-interacting proteins, the top enriched
147 protein (20.8-fold enrichment) was *Pf*EELM2 (PF3D7_0519800). *Pf*EELM2 was previously
148 predicted as a *Pf*MORC interactor (Hillier et al. 2019) and identified in a quantitative histone
149 peptide pulldown to be consistently recruited to H2B.Z_K13/14/18a (Hoeijmakers et al. 2019).
150 Furthermore, we also detected numerous ApiAP2 transcription factors [*Pf*AP2-G5, *Pf*AP2-O5,
151 *Pf*AP2-I, PF3D7_1107800, PF3D7_0613800, PF3D7_0420300 and PF3D7_1239200] (**Table 1**),
152 similar to results reported both by Hillier et al. and with *Toxoplasma Tg*MORC complex (Farhat
153 et al. 2020, Antunes et al. 2023, Srivastava et al. 2023).*Pf*AP2-G5 (PF3D7_1139300) and *Pf*AP2-
154 O5 (PF3D7_1449500) were enriched 20.5- and 14.99-fold, respectively, suggesting that these
155 factors are likely major components in-complex with *Pf*MORC. To corroborate our results, we
156 compared our *Pf*MORC^{GFP} coIPed proteins to a recently published protein–protein network
157 (Hillier et al. 2019, Bryant et al. 2020, Subudhi et al. 2023) and found many of the same ApiAP2
158 and EELM2 proteins across both datasets (**Figure 1B**). Collectively, our results demonstrate a
159 direct association of *Pf*MORC with various chromatin-associated factors, including many
160 ApiAP2 proteins.
161 We also identified proteins implicated in DNA replication and repair, including the ATP-
162 dependent RNA helicase DBP5 (PF3D7_1459000) and the DNA helicase 60 DH60
163 (PF3D7_1227100) associated with *Pf*MORC. PfDH60 exhibits DNA and RNA unwinding
164 activities, and its high expression in the trophozoites suggest a role in DNA replication (Pradhan
165 et al. 2005). We also identified two putative chromatin-associated proteins, chromodomain-
166 helicase-DNA-binding protein 1 CHD1 (PF3D7_1023900) and the SNF2 chromatin-remodeling
167 ATPase ISWI (PF3D7_0624600), which are associated with chromosome structure maintenance,
168 DNA replication, DNA repair, and transcription regulation. PfISWI was previously reported to
169 be associated with *Pf*MORC in the context of transcriptional activation of *var* genes during ring
170 stage development (Bryant et al. 2020). Gene Ontology (GO) analysis was performed to identify
171 enriched biological processes, cellular components, and molecular functions using a p-value cut-
172 off of 0.05. We found significant enrichment of DNA-binding transcription factor activity and
173 mRNA binding, transcription and regulation of transcription activity (**Supplemental Figure 1D,**

174 **Supplemental Table 3)**. Overall, we again find that *Pf*MORC forms a link between ApiAP2 TFs
175 and chromatin remodelers (**Figure 1C**).
176
177 **Table 1 –** Potential *Pf*MORC interacting proteins enriched in CoIP eluates and identified in LC–
178 MS/MS from three independent experiments and fold change ≥ 1.5x GFP/3D7.

Protein ID	Annotation	Fold Change	Known Function
PF3D7_0519800	EELM2 domain-containing protein	20.79	-
PF3D7_1139300	AP2 domain transcription factor AP2-G5	20.5	Repressor of Commitment and Early Gametocyte Development (Shang et al. 2021)
PF3D7_1449500	AP2 domain transcription factor AP2-O5	14.99	Regulator of Mature Ookinete Motility (Modrzynska et al. 2017)
PF3D7_1468100	*Pf*MORC	11.76	
PF3D7_1023900	SNF2 helicase, putative or Chromodomain-helicase-DNA-binding protein 1 homolog, CHD1	10.61	
PF3D7_1459000	ATP-dependent RNA helicase DBP5	10.24	
PF3D7_1227100	DNA helicase 60, DH60	6.55	-
PF3D7_1007700	AP2 domain transcription factor AP2-I	4.65	Invasion (Santos et al. 2017, Josling et al. 2020)
PF3D7_1107800	AP2 domain transcription factor	3.11	Master regulator of parasite growth, chromatin structure and var gene expression (Subudhi et al. 2023)
PF3D7_0613800	AP2 domain transcription factor	2.43	-
PF3D7_0420300	AP2 domain transcription factor (ApiAP2)	2.38	-
PF3D7_0624600	SNF2 helicase, ISW1	2.09	*var* gene expression (Bryant et al. 2020)
PF3D7_1239200	AP2 domain transcription factor	2.01	-

179
180
181 ***PfMORC localizes to multigene families in subtelomeric regions***
182 To determine the genome-wide occupancy of the *Pf*MORC chromatin-associated remodeling
183 complex, we used chromatin immunoprecipitation followed by high-throughput sequencing
184 (ChIP-seq). Using purified, crosslinked nuclear extracts, we immunoprecipitated *Pf*MORC
185 from a 3xHA-tagged *Pf*MORC$^{HA\text{-}glmS}$ parasite line (Singh et al. 2021) for ChIP-seq at the
186 trophozoite stage (30hpi) and the schizont stage (40hpi) in biological duplicates. These
187 timepoints represent the stages at which *Pf*MORC is most highly expressed (Singh et al. 2021).
188 An independent ChIP-seq experiment in biological duplicate using anti-GFP and a *Pf*MORC^{GFP}
189 parasite line (Singh et al. 2021) at the schizont stage was used to confirm our findings,
190 demonstrating that the protein tags do not affect *Pf*MORC immunoprecipitation or genome-
191 wide localization (**Supplemental Figure 2A,B**). As an additional control, we correlated one
192 no-epitope, negative control sample using the same anti-HA antibody on unmodified parasite
193 lines for immunoprecipitation (**Supplemental Figure 2A,B;** (Bonnell et al. 2023)), which
194 resulted in an expected low correlation to the tagged samples. The biological ChIP-seq

195 replicates showed high fold enrichment (Log_2[IP/Input]) (**Supplemental Figure 2C**) and were
196 highly correlated within each timepoint (**Supplemental Figure 2D-F**).
197 We identified PfMORC localized to subtelomeric regions on all chromosomes across the *P.*
198 *falciparum* genome with additional occupancy at internal heterochromatic islands (**Figure**
199 **2A,B**). Within the subtelomeric regions, PfMORC was bound upstream and within the gene
200 bodies of many hypervariable multigene families (**Figure 2C**), including the *var* genes
201 (**Supplemental Figure 3**), *rif* genes (**Supplemental Figure 4**), and *stevor* genes
202 (**Supplemental Figure 5**). Predicted binding sites (across both biological replicates) between
203 the 30hpi and 40hpi timepoints showed a high degree of overlap, suggesting that *Pf*MORC
204 binds many of the same regions throughout the later stages of asexual development when
205 PfMORC is highly expressed (**Figure 2D**). The proportion of *Pf*MORC-bound regions was
206 similar across the 5′ upstream region of genes and the gene bodies throughout the genome,
207 including subtelomeric regions (**Figure 2E**). As opposed to the binding of other proteins at the
208 subtelomeric regions of *P. falciparum*, such as the heterochromatin protein 1 (PfHP1),
209 PfMORC occupancy is not widespread (Flueck et al. 2010). Instead, PfMORC forms sharp
210 peaks within and adjacent to HP1-bound regions (**Figure 2F**), suggesting a unique role for
211 PfMORC in heterochromatin condensation, boundary demarcation, and gene repression.
212 We further defined PfMORC putative gene targets as genes displaying peaks within 2-kb
213 upstream of the ATG start codon or within gene bodies. For those peaks between gene targets
214 in a head-to-head orientation, the closest gene was chosen. This resulted in 149 putative gene
215 targets at 30hpi and 102 gene targets at 40hpi. A close examination of the 84 overlapping genes
216 shows that many are *var*, rRNA, and exported proteins (**Supplemental Table 4**), with GO terms
217 related to cell adhesion, host–pathogen interactions, and antigenic variation (**Supplemental**
218 **Table 5**). The 65 uniquely bound genes at the 30hpi timepoint showed an enrichment of highly
219 expressed tRNA genes, rRNAs, and conserved unknown genes, while those 18 unique to the
220 40hpi timepoint included a variety of late-stage expressed genes. Transcript abundance
221 (Chappell et al. 2020) of the predicted *Pf*MORC gene targets at both the 30hpi and 40hpi
222 timepoints form two major clusters: cluster one being genes expressed at the late ring/early
223 trophozoite stage (10-24hpi) and cluster two at the late schizont stage (40-48hpi)
224 (**Supplemental Figure 6**). This two-cluster gene target pattern of expression mirrors the
225 biphasic pattern of expression by *Pf*MORC, suggesting that *Pf*MORC could have distinct
226 functions, forming complexes with different sets of transcriptional regulators, at various times
227 during asexual proliferation. As determined in other eukaryotic organisms, MORC family
228 proteins do not generally bind DNA in a sequence-specific manner; it is, therefore likely that

229 *Pf*MORC is recruited to these genome-wide regions by sequence-specific transcription factors,
230 such as the ApiAP2 proteins identified in our proteomics results.
231
232 ***Binding sites of PfMORC overlap with ApiAP2 proteins and epigenetic marks***
233 *Pf*MORC has previously been found to interact with several ApiAP2 proteins (Hillier et al.
234 2019, Bryant et al. 2020, Singh et al. 2021), as does the *Toxoplasma* orthologue (Farhat et al.
235 2020, Antunes et al. 2023, Srivastava et al. 2023). We identified the overlap between genome-
236 wide *Pf*MORC binding and putatively interacting ApiAP2 proteins using available ChIP-seq
237 datasets. In addition to our protein-protein interaction results (**Table 1**), previous studies have
238 also suggested that *Pf*MORC interacts with a broad array of ApiAP2 TFs, such as *Pf*AP2-G5 ,
239 *Pf*AP2-O5, *Pf*AP2-I, PF3D7_1107800, PF3D7_0613800, PF3D7_0420300, and
240 PF3D7_1239200 (Hillier et al. 2019, Bryant et al. 2020, Subudhi et al. 2023). Therefore, we
241 compared binding sites between interacting ApiAP2s and *Pf*MORC using available ChIP-seq
242 data on *Pf*AP2-G5, *Pf*AP2-O5, *Pf*AP2-I, PF3D7_1107800, PF3D7_0613800, PF3D7_1239200
243 (Josling et al. 2020, Shang et al. 2021, Shang et al. 2022). Interestingly, there is a degree of
244 overlap between the binding sites of all six ApiAP2 TFs and *Pf*MORC, suggesting that
245 *Pf*MORC and these ApiAP2 TFs may cooperate in the regulation of gene expression at these
246 loci (**Figure 3A-B; Supplemental Figure 7**). However, the available data cannot differentiate
247 whether all of these factors are in one complex together, multiple smaller heterologous
248 complexes, or are components of separate complexes in individual cells. DNA motif enrichment
249 analysis (Bailey 2021) identified several unique and significant DNA motifs at both the 30hpi
250 and 40hpi timepoints, which suggests that more than one sequence-specific transcription factor
251 may be responsible for recruiting *Pf*MORC to specific genomic regions (**Supplemental Figure**
252 **8**). The common motifs identified across replicates and timepoints are RGTGCAW or
253 TGCACACA, which are similar to the *in vitro* and/or *in vivo* DNA-binding motif of *Pf*AP2-I
254 (RGTGCAW) or PF3D7_0420300 (TGCACACA), suggesting that these ApiAP2 factors may
255 play major roles in *Pf*MORC recruitment (**Supplemental Figure 8**).
256 In addition to overlapping occupancy with ApiAP2 TFs, we found that PfMORC co-localizes
257 with the depletion of H3K36me2 (**Figure 3C, D**), which is demarcated by the SET2
258 methyltransferase (Jiang et al. 2013), both at 30hpi and 40hpi. No other significant co-
259 localization was found between PfMORC and other epigenetic marks (H2A.Z, H3K9ac,
260 H3K4me3, H3K27ac, H3K18ac, H3K9me3, H3K36me2/3, H4K20me3, and H3K4me1)
261 (**Supplemental Figure 9**). Therefore, it is likely that PfMORC co-localizes with other, as of
262 yet uncharacterized, epigenetic marks. In summary, *Pf*MORC was found to be recruited to 5`-

263 untranslated regions (UTRs), gene body regions, and subtelomeric regions of repressed,
264 multigene families, and overlaps with other known ApiAP2 binding sites and DNA motifs.
265
266 ***Depletion of PfMORC results in upregulation of late-stage genes associated with invasion***
267 *Pf*MORC association with chromatin remodelers has been shown (Bryant et al. 2020), but how
268 *Pf*MORC regulates gene expression in the asexual stage has not been evaluated. In *T. gondii*,
269 the *Tg*MORC:*Tg*ApiAP2 complex acts as a transcriptional repressor of sexual commitment
270 (Farhat et al. 2020, Antunes et al. 2023, Srivastava et al. 2023). This study found that *Pf*MORC
271 co-immunoprecipitates with several chromatin remodeling proteins and many ApiAP2
272 transcription factors. Furthermore, our ChIP-seq data revealed that *Pf*MORC is located at
273 subtelomeric regions of the genome. Based on this evidence, we hypothesized that PfMORC
274 may regulate transcriptional changes during blood stage development of the parasite. To knock
275 down the expression of *Pf*MORC (*Pf*MORC-KD), sorbitol-synchronized MORC$^{HA\text{-}glmS}$
276 parasites (22-24hpi) were subjected to 2.5 mM glucosamine (GlcN) treatment for little over 48
277 hours when they reached the trophozoite stage (32hpi ± 3hpi), at which point parasites were
278 harvested for RNA isolation for transcriptomic analysis. In parallel, another flask with
279 *Pf*MORC$^{HA\text{-}glmS}$ parasites was set up without GlcN and used as control for RNA-seq
280 comparison. We previously demonstrated that treatment with 2.5 mM GlcN results in a 50%
281 knockdown of *Pf*MORC protein but does not cause any growth delay, however using >2.5 mM
282 GlcN caused a measurable slow growth and reduced parasitemia (Singh et al. 2021). Three
283 biological replicates with and without GlcN were collected for knockdown transcriptomics to
284 ensure reproducibility.
285 For each *Pf*MORC RNA-seq sample, gene counts were ued to identify the differentially
286 expressed genes (DEGs). Significant threshold parameters were assigned to a p value <0.05,
287 yielding a total of 2558 DEGs (**Supplemental Table 6**). Applying a $\log_2$-fold change cut-off
288 from >1 to <-1 and filtering out pseudogenes reduced this number to 163 DEGs. Among these,
289 60 genes display more abundant transcripts, whereas 103 genes were reduced relative to control
290 parasites grown without GlcN **(Figure 4A)**. Pathway and functional enrichment analysis
291 yielded several genes from apical organelles. GO analysis enriched with molecular function (p-
292 adj = 0.0006) which has gene clusters involved in the movement into the host environment and
293 entry into the host, and molecular function of protein binding (p-adj = 0.009) (**Figure 4B,**
294 **Supplemental Table 7)**. More specifically, upregulated genes implicated in the invasion of
295 merozoites were found to be expressed prematurely; these include several rhoptry-associated
296 genes, notably *Pf*RON2 (PF3D7_1452000) and *Pf*RON3 (PF3D7_1252100). Both *Pf*RON2 and

297 *Pf*RON3 are part of a micronemal complex at the erythrocyte membrane where *Pf*RON2
298 anchors *Pf*AMA1 to facilitate merozoite invasion (Srinivasan et al. 2013). In addition, *Pf*SUB3
299 (PF3D7_0507200), *Pf*SERA5 (PF3D7_0207600) and *Pf*DPAP3 (PF3D7_0404700), all of
300 which are critical for schizont rupture (Yeoh et al. 2007, Arastu-Kapur et al. 2008), were among
301 the upregulated DEGs (**Figure 4C**). In general, we found that depletion of *Pf*MORC leads to
302 upregulation of invasion-related genes, which suggests that *Pf*MORC has an additional function
303 in the regulation of genes specifically associated with red blood cell invasion.
304
305 ***PfMORC-depleted parasites downregulate hypervariable gene families***
306 Among the genes with reduced mRNA abundance, DEGs linked to cytoadherence, antigenic
307 variation and interaction with host (**Figure 4B and D**) where over-represented in the GO
308 analysis. Many of the genes enriched in the downregulated group belong to the clonally variant
309 *var* multigene family that represents 60 members encoding the *P. falciparum* erythrocyte
310 membrane proteins (PfEMP1), which upon switching expression, aid in pathogenesis and
311 immune evasion (Guizetti and Scherf 2013). Furthermore, a cluster of genes encoding putative
312 exported proteins were also enriched including members of the exported protein family (EPFs),
313 *Plasmodium* exported protein (hyp), and *Plasmodium* exported protein (PHISTa/b). Other
314 significantly overrepresented downregulated genes belonged to serine/threonine protein
315 kinases, the FIKK family (Ward et al. 2004) and Maurer's clefts two transmembrane proteins
316 (Pfmc-2TM) (**Figure 4 D**). Notably, expressed proteins are conserved across the *Plasmodium*
317 family and remain confined to the hypervariable subtelomeric region of *P. falciparum*
318 chromosomes (Sargeant et al. 2006).
319
320 ***Comparison of ChIP-seq gene targets and DEGs by RNA-seq***
321 To identify whether genes found to be dysregulated after PfMORC knockdown are associated
322 with the genome-wide occupancy of PfMORC, we correlated the gene targets identified by
323 ChIP-seq with the DEGs determined by RNA-seq. We identified a total of 135 gene targets
324 from the 30hpi ChIP-seq timepoint, 72 gene targets from the 40hpi ChIP-seq timepoint, and
325 163 DEGs by RNA-seq. The low correlation between the ChIP-seq gene targets and the RNA-
326 seq DEGs suggest that PfMORC genome-wide occupancy is more likely involved in chromatin
327 structure, rather than specific regulation of gene targets (**Figure 4E**). Likely, PfMORC localizes
328 to these sites to aid in chromatin condensation, as shown in other eukaryotic systems (Zhang et
329 al. 2019, Zhong et al. 2023).
330

Discussion

Periodic gene expression during the asexual blood stage directly corresponds to the timing in which gene products are needed (Bozdech et al. 2003) and shows oscillation patterns associated with circadian rhythms (Smith et al. 2020, Subudhi et al. 2020). Transcription factors are critical regulators of this dynamic pattern in concert with epigenetic regulators and genome-wide changes to chromatin structure (Painter et al. 2011, Toenhake et al. 2018, Jeninga et al. 2019, Hollin et al. 2021). The ApiAP2 family members undergo unique binding preferences in the genome (Campbell et al. 2010), display stage-specific expression (Painter et al. 2011), and have been identified to regulate virtually all stages of development across multiple *Plasmodium* species (Jeninga et al. 2019). To date, ApiAP2 proteins have been reported in the transcriptional silencing of clonally variant genes, regulation of invasion genes, and sexual commitment by interaction with other epigenetic factors, such as heterochromatin protein 1 [*Pf*HP1 (Flueck et al. 2010, Brancucci et al. 2014, Fraschka et al. 2018)], bromodomain protein 1 [*Pf*BDP1 (Santos et al. 2017, Josling et al. 2020, Quinn et al. 2022)], or general control non-depressible 5 [PfGCN5 (Miao et al. 2021)]. Despite the known DNA-binding sites of many ApiAP2 proteins (Flueck et al. 2010, Santos et al. 2017, Sierra-Miranda et al. 2017, Josling et al. 2020, Carrington et al. 2021, Shang et al. 2021, Singh et al. 2021, Russell et al. 2022, Shang et al. 2022, Bonnell et al. 2023), limited information is available for other accessory proteins. Recently, *Tg*MORC was identified in a complex with HDAC1, AP2XII-2, and AP2XII-1:AP2XI-2 in *T. gondii* and orchestrates epigenetic rewiring of sexual gene transcription (Farhat et al. 2020, Antunes et al. 2023, Srivastava et al. 2023). In *P. falciparum*, *Pf*MORC has been copurified with several ApiAP2 proteins, as shown by different independent studies (Hillier et al. 2019, Bryant et al. 2020, Singh et al. 2021).

In this study, we used an integrated multi-omics approach to explore the function of *Pf*MORC during asexual blood stage development. We identified a number of nuclear proteins that interact with *Pf*MORC using immunoaffinity-based purification. More specifically, *Pf*MORC was associated with *Pf*AP2-G5, which is essential for gametocytogenesis (Shang et al. 2021), *Pf*AP2-I, which is required for the expression of many invasion-related genes (Santos et al. 2017), and with other ApiAP2 TFs of unknown function during the asexual blood stage of development (*Pf*AP2-O5, PF3D7_1107800, PF3D7_0613800, PF3D7_0420300, and PF3D7_1239200). The identification of *Pf*ISW1 and *Pf*CHD1 in association with *Pf*MORC strengthens the link between *Pf*MORC and a role in chromatin remodeling. This finding suggests that *Pf*MORC may participate in regulating chromatin structure, gene expression

364 during the IDC, and in the specific regulation of *var* genes, which are critical to antigenic
365 variation in *P. falciparum*. We note that some nuclear proteins were not identified in this study
366 despite their expected interaction with *Pf*MORC as shown in other studies (Hillier et al. 2019,
367 Bryant et al. 2020, Singh et al. 2021, Subudhi et al. 2023). This may be due to limitations in the
368 experimental conditions and low abundance of the proteins. Despite this, the identification of
369 these nuclear proteins in complex with *Pf*MORC provides insights into potential interactions
370 and regulatory mechanisms involved in molecular mechanisms underlying gene regulation and
371 chromatin remodeling in *P. falciparum*, which may have implications for developing new
372 strategies to combat malaria.
373 In other eukaryotic organisms, MORC family proteins are known to function in gene repression
374 and chromatin compaction at heterochromatic regions (Koch et al. 2017). Therefore, to
375 determine if *Pf*MORC localizes to heterochromatic regions across the *P. falciparum* genome,
376 we performed ChIP-seq assays with MORC$^{HA\text{-}glmS}$ parasites during peak PfMORC expression
377 (trophozoite and schizont stages). In general, *Pf*MORC occupied regions 5`–upstream of the
378 ATG start site or bound within coding region, irrespective of the parasite stage. Most
379 importantly, *Pf*MORC peaks were reproducibly detected in subtelomeric regions containing
380 hypervariable multigene families, including the *var* genes, thereby confirming the findings that
381 *Pf*MORC localized to *var* gene promoters as reported using dCas9 (Bryant et al. 2020). The
382 specific binding pattern of *Pf*MORC near or within *Pf*HP1-bound regions suggests two critical
383 functions: heterochromatin condensation and gene repression. It is possible that *Pf*MORC
384 changes the nucleosome landscape by either direct association or by binding to different
385 chromatin remodelers. Recent work in *Arabidopsis* has further confirmed the importance of
386 *At*MORC paralogs in gene regulation by chromatin compaction (Zhong et al. 2023), which
387 resembles the function of *Pf*MORC in *P. falciparum*. Interestingly, in *T. gondii*, the major
388 function of *Tg*MORC was in the repression of sex-determination genes (Farhat et al. 2020),
389 suggesting MORC family proteins have the capacity to perform diverse functions across
390 eukaryotic organisms.
391 Based on our immunoprecipitation results, we compared *Pf*MORC occupancy with available
392 ChIP-seq data for the interacting ApiAP2 proteins. Interestingly, our analysis revealed a
393 significant overlap between the binding sites of all ChIP-ed ApiAP2 proteins with *Pf*MORC,
394 suggesting a cooperative role in gene regulation. We also identified enriched motifs similar to
395 those bound by our ApiAP2 proteins of interest, further suggesting the functional cooperation
396 between PfMORC and ApiAP2 proteins. Of note, only one of the seven ApiAP2 of interest in
397 our study has not been ChIP-ed to date (PF3D7_0420300) (Shang et al. 2022). However, we

398 found an enrichment of the DNA motif (TGCACACA) at PfMORC-bound sites. This motif is
399 bound *in vitro* by PF3D7_0420300 (Bonnell et al. 2023) suggesting that this ApiAP2 protein
400 may localize to these regions. Overall, since these seven ApiAP2 proteins are expressed at
401 distinct time points during the *P. falciparum* cycle (Bozdech et al. 2003) and regulate different
402 sets of genes (Santos et al. 2017, Josling et al. 2020, Shang et al. 2021, Shang et al. 2022,
403 Subudhi et al. 2023), we believe this indicates a broad function of *Pf*MORC at different stages.
404 In addition, a recent study reported that *At*MORC-mediated regulation of transcription may be
405 due to both direct chromatin interactions or indirect association via sequence-specific
406 transcription factors (Zhong et al. 2023), suggesting a complex landscape of chromatin
407 remodeling by MORC family proteins. We also interrogated the co-localization of *Pf*MORC
408 and numerous epigenetic profiles (H2A.Z, H3K9ac, H3K4me3, H3K27ac, H3K18ac,
409 H3K9me3, H3K36me2/3, H4K20me3, and H3K4me1), with a specific focus on H3K36me2,
410 since it has been shown to act as a global repressive mark in *P. falciparum* (Karmodiya et al.
411 2015) and other organisms (Strahl et al. 2002, Wagner and Carpenter 2012). Interestingly, we
412 did not find a strong co-localization with any of these epigenetic marks, suggesting a unique
413 role of the epigenetic landscape on PfMORC global occupancy. Therefore, the functional
414 association between *Pf*MORC and a specific, unknown epigenetic mark remains to be
415 determined.
416 Previous to this work, there was no direct evidence correlating *Pf*MORC-mediated
417 transcriptional changes during the IDC of *P. falciparum*. Therefore, we investigated the
418 differentially expressed genes (DEGs) in *Pf*MORC knockdown parasites and found two distinct
419 subsets of genes that were enriched. The upregulated DEGs were enriched with genes related
420 to invasion, with downregulated DEGs belonging to hypervariable genes associated with
421 parasite virulence. Upregulation of invasion genes after depletion of PfMORC, along with the
422 putative interaction we identified with PfAP2-I, is particularly interesting as it provides further
423 understanding of the essential red blood cell invasion step of parasite development. Overall, our
424 data with *Pf*MORC-KD revealed a change in the expression of both antigenically variable and
425 invasion-related genes. Expression of clonally variant genes occurs in a different but tightly
426 regulated manner in IDC (Scherf et al. 1998, Scherf et al. 2008), which may be regulated by
427 PfMORC occupancy. Data regarding changes in var genes expression are difficult to interpret,
428 as the KD experiments were performed on a parasite that had not be recently recloned and may
429 therefore express various var genes; single-cell experiments would be needed to clarify the
430 effect of PfMORC KD on var gene regulation.

431 The Garcia group showed previously that parasites in which PfMORC is knocked-down display
432 reduced sensitivity to melatonin (Singh et al. 2021). This prompted us to investigate if overall
433 gene expression in PfMORC KD parasites is affected by melatonin treatment. We detected only
434 very slight changes **(Supplemental Figure 10A-D)**, suggesting that melatonin does not exert
435 its effect on gene expression through PfMORC, or at least that the latter protein plays a minor
436 role in the process.
437 This study shows that *Pf*MORC interacts with different ApiAP2 TFs, as demonstrated in
438 previous studies (Hillier et al. 2019, Bryant et al. 2020, Singh et al. 2021, Subudhi et al. 2023).
439 Furthermore, we found that *Pf*MORC is localized at sub-telomeric regions and contains
440 significant overlap with the binding sites of several ApiAP2 transcription factors. Our results
441 support a role for *Pf*MORC in the regulation of hypervariable genes that are essential for
442 *Plasmodium* virulence and rhoptry genes critical to red blood cell invasion. Collectively, our
443 data identify an important role for *Pf*MORC in chromatin organization, as well as in the
444 epigenetic regulation of gene expression through regulatory complexes with an array of
445 transcription factors, making it an attractive drug target.

446 # Materials and Methods

447 ***Plasmodium falciparum* culture**

448 The *P. falciparum* strains were cultured at 37°C in RPMI 1640 medium supplemented with
449 0.5% Albumax II (Gibco) (Trager and Jensen 1976). Parasites were grown under a 5% CO_2,
450 5% O_2, and 90% N_2 atmosphere. Cultures were synchronized with 5% sorbitol (Lambros and
451 Vanderberg 1979).

452

453 **Coimmunoprecipitation and mass spectrometry**

454 Infected erythrocytes at the trophozoite stage were collected from culture and washed twice in
455 1x phosphate-buffered saline (PBS). The culture pellet was suspended in PBS containing 0.05%
456 (w/v) saponin to lyse the erythrocyte membrane and centrifuged at 8,000 × g for 10 min. The
457 supernatant was discarded, and the parasite pellet was washed 3 times in cold PBS. Samples
458 were lysed in modified RIPA buffer (50 mM Tris, pH 7.5, 150 mM NaCl, 0.5% sodium
459 deoxycholate, 1% Nonidet P-40, 10 µg/ml aprotinin, 10 µg/ml leupeptin, 10 µg/ml, 1 mM
460 phenylmethylsulfonyl fluoride, benzamidine) for 30 min on ice. The lysate was precleared with
461 50 µl of protein A/G-Agarose beads at 4 °C for 1 h and clarified by centrifugation at 10,000 ×
462 g for 10 min. The precleared lysate was incubated with an anti-GFP-Trap-A beads (ChromoTek,
463 gta-20) antibody overnight. The magnetic beads were then pelleted using a magnet (Invitrogen),
464 and the beads were washed extensively. To elute the immunoprecipitated proteins, the magnetic
465 beads were resuspended in 2X SDS loading buffer and resolved by SDS–PAGE. Following
466 SDS–PAGE, the whole gel band for each sample was excised and further analysed by mass
467 spectrometry. We used a service provider (CEFAP core-facility de Espectometria de Massa) to
468 analyse GFP-coimmunoprecipitated proteins.

469

470 **In-gel digestion and peptide desalting**

471 Protein bands from polyacrylamide gel were cut into pieces (approximately 1 mm^3), transferred
472 to a clean 1.5 ml low binding tube and washed with washing solution (40% acetonitrile, 50 mM
473 ammonium bicarbonate) until the bands were completely distained and dehydrated with ACN
474 100% for 5 min followed by vacuum centrifugation. Proteins were then reduced with 10 mM
475 dithiothreitol (DTT) in 50 mM ammonium bicarbonate and incubated for 45 minutes at 56 °C.
476 Protein alkylation was performed with 55 mM iodoacetamide (IAA) in 50 mM ammonium
477 bicarbonate and incubated for 30 minutes at room temperature. Proteins were digested into
478 peptides by trypsin overnight reaction at 37 °C. The trypsin reaction was stopped with 10%

479 TFA (1% TFA final concentration). The supernatant was collected into a new tube. Extraction
480 buffer (40% ACN/0.1% TFA) was added to the gel pieces and incubated for 15 minutes on a
481 thermomixer at room temperature. The supernatant was transferred to the same microtube. The
482 peptide extraction was performed twice and then dried in a vacuum centrifuge. Peptides were
483 resuspended in 0.1% TFA for desalting.
484

485 **Nano LC–MS/MS analysis**

486 The LC–MS/MS system employed was an Easy-nano LC 1200 system (Thermo Fisher
487 Scientific Corp) coupled to an Orbitrap Fusion Lumos mass spectrometer equipped with a
488 nanospray source (Thermo Fisher Scientific Corp). Samples were loaded onto a trapping
489 column (Acclaim PepMap 0.075 mm, 2 cm, C18, 3 µm, 100 A; Thermo Fisher Scientific Corp.)
490 in line with a nano-LC column (Acclaim PepMap RSLC 0.050 mm, 15 cm, C18, 2 µm, 100 A;
491 Thermo Fisher Scientific Corp.). The gradient was 5-28% solvent B (A 0.1% FA; B 90% ACN,
492 0.1% FA) for 25 minutes, 28-40% B for 3 minutes, 40-95% B for 2 minutes and 95% B for 12
493 minutes at 300 nL/min. Orbitrap Fusion Lumos mass spectrometer operated in positive mode.
494 The full MS scan had an automatic gain control (AGC) of 5 x 105 ions and a maximum filling
495 time of 50 ms. Each MS scan was acquired at 120K full width half maximum (FWHM) high
496 resolution in the Orbitrap with a mass range of m/z 400-1600 Da. High-resolution dissociation
497 (HCD) with a normalized collision energy set at 30 was used for fragmentation. The resulting
498 MS/MS fragment ions were detected in the Orbitrap mass analyser at a resolution of 30,000.
499 An AGC of 5 x 104 ions and a maximum injection time of 54 ms were used. All raw data were
500 accessed in Xcalibur software (Thermo Scientific).
501

502 **Database searches and bioinformatics analyses**

503 Raw files were imported into MaxQuant version 1.6.17.0 for protein identification and
504 quantification. For protein identification in MaxQuant, the database search engine Andromeda
505 was used against the UniProt *P. falciparum* 3D7 strain (March 2021, 5388 entries release). The
506 following parameters were used: carbamidomethylation of cysteine (57.021464 Da) as a fixed
507 modification, oxidation of methionine (15.994915 Da) and N-terminal acetylation protein
508 (42.010565 Da) were selected as variable modifications. Enzyme specificity was set to full
509 trypsin with a maximum of two missed cleavages. The minimum peptide length was set to 7
510 amino acids. For label-free quantification, the "match between runs" feature in MaxQuant was
511 used, which is able to identify the transfer between samples based on the retention time and
512 accurate mass, with a 0.7-minute match time window and 20-minute alignment time window.

513 Label-free quantification was performed using MaxQuant software with the "match between
514 run" and iBAQ features activated. Protein LFQ and iBAQ ratios were calculated for the two
515 conditions, and the protein IDs were divided accordingly. The mass spectrometry proteomics
516 data have been deposited to the ProteomeXchange Consortium via the PRIDE (Perez-Riverol
517 et al. 2022) partner repository with the dataset identifier PXD036092. PlasmoDB database was
518 used to perform GO analysis.
519
520 **Total RNA extraction and RNAseq**
521 Infected RBCs containing tightly synchronized trophozoite stage parasites (32 hpi ± 3 h) were
522 harvested and resuspended in TRIzol (Thermo Fisher Scientific). Total RNA was extracted
523 following the manufacturer's protocol, and an RNA cleanup kit (Qiagen) was used to achieve
524 high-purity RNA. The isolated RNA was quantified using a NanoDrop ND-1000 UV/Vis
525 spectrophotometer, and RNA quality was determined using an RNA ScreenTape System
526 (Agilent 2200 TapeStation). Total RNA (10000 ng) from each sample was stabilized in
527 RNAStable (Biomatrica) and sent to the Micromon Genomics facility at Monash University for
528 next-generation sequencing.
529 RNA samples were prepared using the MGITech RNA Directional Library Prep Kit V2 (Item
530 No. 1000006385), as per the manufacturer's instructions, with the following parameters: input
531 RNA: 50 ng, fragmentation: target of 200 bp-400 bp, 87 °C for 6 mins, adapter clean-up: 200
532 bp-400 bp and library amplification cycles: 16. Libraries were assessed for quantity using the
533 Invitrogen Qubit and dsDNA HS chemistry (Item No. Q33230) and quality/quality using the
534 Agilent Fragment Analyser 5200 with the HS NGS Fragment Kit (Item No. DNF-473-0500).
535 The libraries were pooled in equimolar concentrations and sequenced using an MGITech
536 DNBSEQ-G400RS sequencing instrument with High-Throughput Sequencing Set (FCL
537 PE100, Item No. 1000016950) chemistry.
538 The quality of the RNA-seq libraries was evaluated using the FastQC tool. Next, we used
539 Salmon (V1.9.0) (Patro et al. 2017) quant with default arguments to quantify the expression of
540 all transcripts in the PlasmoDB release-58 Pfalciparum3D7 genome. The transcript expression
541 was summarized to gene-level expression with tximport 1.22.0 (Soneson et al. 2015). Finally,
542 the gene counts were used to detect differentially expressed genes (DEGs) with DESeq2
543 (1.34.0) (Love et al. 2014). Furthermore, only genes with an >1 $\log_2$ fold change and adjusted
544 p value <0.1 were considered significant for further analysis.
545
546 **Chromatin immunoprecipitation followed by high-throughput sequencing (ChIP-seq)**

547 PfMORC ChIP-seq was performed similarly to previously published ChIP-seq experiments in
548 *Plasmodium falciparum* (Josling et al. 2020, Singh et al. 2021, Russell et al. 2022). Five
549 samples in total were collected: biological duplicates using the PfMORC$^{HA\text{-}glmS}$ parasite line at
550 the trophozoite stage [30 hpi], biological duplicates using the PfMORC^{HA} parasite line at the
551 schizont stage [40 hpi], and a single replicate using the PfMORC^{GFP} parasite line at the schizont
552 stage [40 hpi]. In brief, the protocol includes five steps: (1) Treated with 1% formaldehyde to
553 crosslink the suspended PfMORC$^{HA\text{-}glmS}$ (or PfMORC^{GFP}) parasite cultures (at least 10^8
554 trophozoite- or schizont-stage parasites synchronized with 10% sorbitol more than one cycle
555 prior) at 37°C for 10 minutes; (2) Collected parasite nuclei using prechilled glass dounce
556 homogenizer for 100 strokes per 10^9 trophozoites/schizonts; (3) Lysed parasite nuclei and
557 mechanically sheared chromatin until sufficiently sheared using Covaris Focus-Ultrasonicator
558 M220 (5% duty cycle, 75 W peak incident power, 200 cycles per burst, 7°C, for 5 minutes). (4)
559 We collected 10% of each sample for the nonimmunoprecipitated "input" control and then
560 immunoprecipitated the remaining 90% of each sample. The remaining 90% of each sample
561 was immunoprecipitated with 1:1000 anti-HA antibody (0.5 mg/mL Roche Rat Anti-HA High
562 Affinity [11867423001]) or 1:1000 anti-GFP antibody (0.1 mg/mL Abcam Rabbit Anti-GFP
563 [Ab290]) overnight at 4°C with rotation. (5) DNA was purified after reverse crosslinking using
564 a MinElute column (Qiagen) as directed and quantified by a Qubit fluorometer (Invitrogen).
565
566 **ChIP-seq library prep for Illumina sequencing**
567 The PfMORC ChIP-seq libraries were performed similarly to previously published ChIP-seq
568 experiments in *Plasmodium falciparum* (Josling et al. 2020, Singh et al. 2021, Russell et al.
569 2022). DNA sequencing libraries were prepared for high-throughput Illumina sequencing on
570 the NextSeq 2000 with the 150 x 150 single-end mode. The library prep underwent 12 rounds
571 of amplification using KAPA HiFi polymerase. Completed libraries were quantified using the
572 Qubit fluorometer (Invitrogen) for high-sensitivity DNA and library sequence length by the
573 Agilent TapeStation 4150.
574
575 **ChIP-seq data analysis and peak calling**
576 The MORC ChIP-seq datasets were analysed similar to previously published ChIP-seq
577 experiments in *Plasmodium falciparum* (Josling et al. 2020, Singh et al. 2021, Russell et al.
578 2022). Raw sequencing reads were trimmed (Trimmomatic v0.32.3) to remove Illumina adaptor
579 sequences and low-quality reads below 30 Phred (SLIDINGWINDOW: 4:30). FastQC
580 (v0.11.9) was used to check the quality after trimming. Processed reads were then mapped to

581 the *P. falciparum* genome (release 57) using BWA-MEM (v0.7.17.2) simple Illumina mode
582 with multiple mapped reads filtered out (MAPQ=1). Once the sequences were mapped, MACS2
583 (v2.2.7.1) was used to call peaks with each biological replicate and its paired input sample using
584 a standard significance cut-off (q-value=0.01). Using BedTools Multiple Intersect (v2.29.2),
585 the narrow peak output file for each replicate was overlapped to identify the significant peaks
586 in the overlap between both ChIP-seq biological replicates. The overlapping regions were then
587 used to identify an enriched DNA motif (STREME Meme Suite: (Bailey 2021), and putative
588 gene targets of PfMORC were defined as genes with peaks within 2 kb upstream of the gene
589 target ATG start codon or peaks within gene bodies. In a situation with any peaks between gene
590 targets in a head-to-head orientation, the closest gene was chosen.

Data availability

The mass spectrometry proteomics data have been deposited to the ProteomeXchange Consortium via the PRIDE partner repository with the dataset identifier PXD044256. All ChIP-seq samples were submitted to GEO, and a GEO submission ID (GSE239393) was obtained for this section. Additionally, submit all the relevant ChIP-seq files to Zenodo, since UCSC browser doesn't easily work from *Plasmodium falciparum* data. All RNA-seq samples were submitted to GEO, and a GEO submission ID (GSE241313) was obtained for this section.

Author Contributions

MKS, CRSG, and ML designed the experiments. MKS, VAB, VFS and MSM performed the experiments, and data were analyzed by MKS, VAB, ITS, GP, ML and CRSG. The primary manuscript was written by MKS and VAB and proofread by CD, ML and CRSG.

Acknowledgements

This work was supported by grants from Fundação de Amparo a Pesquisa de São Paulo (FAPESP) to CRSG (2017/08684-7 and 2018/07177-7) and to MKS (2019/09490-7). CRSG is supported by "bolsa de produtividade" by CNPq. This work was supported by the National Institutes of Health grant number R01-AI125565 to M.L. and T32-GM125592 to V.A.B. We are grateful to Haemocentro Hospital do Servidor Público for providing blood and plasma. Work in CD laboratory is supported by RMIT University and by grant APP2003712 from the Australian Health and Medical Research Council (NHMRC).

Additional Information

Additional figures and tables are provided separately in Supplemental Figures and Supplemental Tables.

Competing Financial Interests

The authors declare no competing financial interests.

619 **References**

620 Antunes, A. V., M. Shahinas, C. Swale, D. C. Farhat, C. Ramakrishnan, C. Bruley, D. Cannella, C. Corrao,
621 Y. Couté, A. B. Hehl, A. Bougdour, I. Coppens and M.-A. Hakimi (2023). "*In vitro* production of cat-
622 restricted *Toxoplasma* pre-sexual stages by epigenetic reprogramming." bioRxiv:
623 2023.2001.2016.524187.
624 Arastu-Kapur, S., E. L. Ponder, U. P. Fonovic, S. Yeoh, F. Yuan, M. Fonovic, M. Grainger, C. I. Phillips, J.
625 C. Powers and M. Bogyo (2008). "Identification of proteases that regulate erythrocyte rupture by the
626 malaria parasite Plasmodium falciparum." Nat Chem Biol **4**(3): 203-213.
627 Bailey, T. L. (2021). "STREME: Accurate and versatile sequence motif discovery." Bioinformatics **37**(18):
628 2834-2840.
629 Balaji, S., M. M. Babu, L. M. Iyer and L. Aravind (2005). "Discovery of the principal specific transcription
630 factors of Apicomplexa and their implication for the evolution of the AP2-integrase DNA binding
631 domains." Nucleic Acids Res **33**(13): 3994-4006.
632 Bonnell, V. A., Y. Zhang, J. Alan S. Brown, J. Horton, G. A. Josling, T.-P. Chiu, R. Rohs, S. Mahony, R.
633 Gordân and M. Llinás (2023). "DNA sequence context and the chromatin landscape differentiate
634 sequence-specific transcription factor binding in the human malaria parasite, Plasmodium
635 falciparum." bioRxiv: 2023.2003.2031.535174.
636 Bordiya, Y., Y. Zheng, J. C. Nam, A. C. Bonnard, H. W. Choi, B. K. Lee, J. Kim, D. F. Klessig, Z. Fei and H.
637 G. Kang (2016). "Pathogen Infection and MORC Proteins Affect Chromatin Accessibility of Transposable
638 Elements and Expression of Their Proximal Genes in Arabidopsis." Mol Plant Microbe Interact **29**(9):
639 674-687.
640 Bozdech, Z., M. Llinas, B. L. Pulliam, E. D. Wong, J. Zhu and J. L. DeRisi (2003). "The transcriptome of
641 the intraerythrocytic developmental cycle of Plasmodium falciparum." PLoS Biol **1**(1): E5.
642 Brancucci, N. M. B., N. L. Bertschi, L. Zhu, I. Niederwieser, W. H. Chin, R. Wampfler, C. Freymond, M.
643 Rottmann, I. Felger, Z. Bozdech and T. S. Voss (2014). "Heterochromatin protein 1 secures survival and
644 transmission of malaria parasites." Cell Host Microbe **16**(2): 165-176.
645 Bryant, J. M., S. Baumgarten, F. Dingli, D. Loew, A. Sinha, A. Claes, P. R. Preiser, P. C. Dedon and A.
646 Scherf (2020). "Exploring the virulence gene interactome with CRISPR/dCas9 in the human malaria
647 parasite." Mol Syst Biol **16**(8): e9569.
648 Budu, A., R. Peres, V. B. Bueno, L. H. Catalani and C. R. Garcia (2007). "N1-acetyl-N2-formyl-5-
649 methoxykynuramine modulates the cell cycle of malaria parasites." J Pineal Res **42**(3): 261-266.
650 Bushell, E., A. R. Gomes, T. Sanderson, B. Anar, G. Girling, C. Herd, T. Metcalf, K. Modrzynska, F.
651 Schwach, R. E. Martin, M. W. Mather, G. I. McFadden, L. Parts, G. G. Rutledge, A. B. Vaidya, K.
652 Wengelnik, J. C. Rayner and O. Billker (2017). "Functional Profiling of a Plasmodium Genome Reveals
653 an Abundance of Essential Genes." Cell **170**(2): 260-272 e268.
654 Campbell, T. L., E. K. De Silva, K. L. Olszewski, O. Elemento and M. Llinas (2010). "Identification and
655 genome-wide prediction of DNA binding specificities for the ApiAP2 family of regulators from the
656 malaria parasite." PLoS Pathog **6**(10): e1001165.
657 Carrington, E., R. H. M. Cooijmans, D. Keller, C. G. Toenhake, R. Bartfai and T. S. Voss (2021). "The
658 ApiAP2 factor PfAP2-HC is an integral component of heterochromatin in the malaria parasite
659 Plasmodium falciparum." iScience **24**(5): 102444.
660 Chappell, L., P. Ross, L. Orchard, T. J. Russell, T. D. Otto, M. Berriman, J. C. Rayner and M. Llinas (2020).
661 "Refining the transcriptome of the human malaria parasite Plasmodium falciparum using amplification-
662 free RNA-seq." BMC Genomics **21**(1): 395.
663 Cowman, A. F., D. Berry and J. Baum (2012). "The cellular and molecular basis for malaria parasite
664 invasion of the human red blood cell." J Cell Biol **198**(6): 961-971.
665 Dong, W., A. Vannozzi, F. Chen, Y. Hu, Z. Chen and L. Zhang (2018). "MORC Domain Definition and
666 Evolutionary Analysis of the MORC Gene Family in Green Plants." Genome Biol Evol **10**(7): 1730-1744.
667 Farhat, D. C., C. Swale, C. Dard, D. Cannella, P. Ortet, M. Barakat, F. Sindikubwabo, L. Belmudes, P. J.
668 De Bock, Y. Coute, A. Bougdour and M. A. Hakimi (2020). "A MORC-driven transcriptional switch

controls Toxoplasma developmental trajectories and sexual commitment." Nat Microbiol **5**(4): 570-583.
Flueck, C., R. Bartfai, I. Niederwieser, K. Witmer, B. T. Alako, S. Moes, Z. Bozdech, P. Jenoe, H. G. Stunnenberg and T. S. Voss (2010). "A major role for the Plasmodium falciparum ApiAP2 protein PfSIP2 in chromosome end biology." PLoS Pathog **6**(2): e1000784.
Fraschka, S. A., M. Filarsky, R. Hoo, I. Niederwieser, X. Y. Yam, N. M. B. Brancucci, F. Mohring, A. T. Mushunje, X. Huang, P. R. Christensen, F. Nosten, Z. Bozdech, B. Russell, R. W. Moon, M. Marti, P. R. Preiser, R. Bartfai and T. S. Voss (2018). "Comparative Heterochromatin Profiling Reveals Conserved and Unique Epigenome Signatures Linked to Adaptation and Development of Malaria Parasites." Cell Host Microbe **23**(3): 407-420 e408.
Gardner, M. J., N. Hall, E. Fung, O. White, M. Berriman, R. W. Hyman, J. M. Carlton, A. Pain, K. E. Nelson, S. Bowman, I. T. Paulsen, K. James, J. A. Eisen, K. Rutherford, S. L. Salzberg, A. Craig, S. Kyes, M. S. Chan, V. Nene, S. J. Shallom, B. Suh, J. Peterson, S. Angiuoli, M. Pertea, J. Allen, J. Selengut, D. Haft, M. W. Mather, A. B. Vaidya, D. M. Martin, A. H. Fairlamb, M. J. Fraunholz, D. S. Roos, S. A. Ralph, G. I. McFadden, L. M. Cummings, G. M. Subramanian, C. Mungall, J. C. Venter, D. J. Carucci, S. L. Hoffman, C. Newbold, R. W. Davis, C. M. Fraser and B. Barrell (2002). "Genome sequence of the human malaria parasite Plasmodium falciparum." Nature **419**(6906): 498-511.
Guizetti, J. and A. Scherf (2013). "Silence, activate, poise and switch! Mechanisms of antigenic variation in Plasmodium falciparum." Cell Microbiol **15**(5): 718-726.
Harris, M. T., V. Jeffers, J. Martynowicz, J. D. True, A. L. Mosley and W. J. Sullivan, Jr. (2019). "A novel GCN5b lysine acetyltransferase complex associates with distinct transcription factors in the protozoan parasite Toxoplasma gondii." Mol Biochem Parasitol **232**: 111203.
Hillier, C., M. Pardo, L. Yu, E. Bushell, T. Sanderson, T. Metcalf, C. Herd, B. Anar, J. C. Rayner, O. Billker and J. S. Choudhary (2019). "Landscape of the Plasmodium Interactome Reveals Both Conserved and Species-Specific Functionality." Cell Rep **28**(6): 1635-1647 e1635.
Hoeijmakers, W. A. M., J. Miao, S. Schmidt, C. G. Toenhake, S. Shrestha, J. Venhuizen, R. Henderson, J. Birnbaum, S. Ghidelli-Disse, G. Drewes, L. Cui, H. G. Stunnenberg, T. Spielmann and R. Bartfai (2019). "Epigenetic reader complexes of the human malaria parasite, Plasmodium falciparum." Nucleic Acids Res **47**(22): 11574-11588.
Hollin, T., M. Gupta, T. Lenz and K. G. Le Roch (2021). "Dynamic Chromatin Structure and Epigenetics Control the Fate of Malaria Parasites." Trends Genet **37**(1): 73-85.
Hotta, C. T., M. L. Gazarini, F. H. Beraldo, F. P. Varotti, C. Lopes, R. P. Markus, T. Pozzan and C. R. Garcia (2000). "Calcium-dependent modulation by melatonin of the circadian rhythm in malarial parasites." Nat Cell Biol **2**(7): 466-468.
Iyer, L. M., S. Abhiman and L. Aravind (2008). "MutL homologs in restriction-modification systems and the origin of eukaryotic MORC ATPases." Biol Direct **3**: 8.
Iyer, L. M., V. Anantharaman, M. Y. Wolf and L. Aravind (2008). "Comparative genomics of transcription factors and chromatin proteins in parasitic protists and other eukaryotes." Int J Parasitol **38**(1): 1-31.
Jeninga, M. D., J. E. Quinn and M. Petter (2019). "ApiAP2 Transcription Factors in Apicomplexan Parasites." Pathogens **8**(2).
Jiang, L., J. Mu, Q. Zhang, T. Ni, P. Srinivasan, K. Rayavara, W. Yang, L. Turner, T. Lavstsen, T. G. Theander, W. Peng, G. Wei, Q. Jing, Y. Wakabayashi, A. Bansal, Y. Luo, J. M. Ribeiro, A. Scherf, L. Aravind, J. Zhu, K. Zhao and L. H. Miller (2013). "PfSETvs methylation of histone H3K36 represses virulence genes in Plasmodium falciparum." Nature **499**(7457): 223-227.
Josling, G. A., T. J. Russell, J. Venezia, L. Orchard, R. van Biljon, H. J. Painter and M. Llinas (2020). "Dissecting the role of PfAP2-G in malaria gametocytogenesis." Nat Commun **11**(1): 1503.
Kafsack, B. F., N. Rovira-Graells, T. G. Clark, C. Bancells, V. M. Crowley, S. G. Campino, A. E. Williams, L. G. Drought, D. P. Kwiatkowski, D. A. Baker, A. Cortes and M. Llinas (2014). "A transcriptional switch underlies commitment to sexual development in malaria parasites." Nature **507**(7491): 248-252.
Kang, H. G., W. C. Hyong, S. von Einem, P. Manosalva, K. Ehlers, P. P. Liu, S. V. Buxa, M. Moreau, H. G. Mang, P. Kachroo, K. H. Kogel and D. F. Klessig (2012). "CRT1 is a nuclear-translocated MORC endonuclease that participates in multiple levels of plant immunity." Nat Commun **3**: 1297.

721 Karmodiya, K., S. J. Pradhan, B. Joshi, R. Jangid, P. C. Reddy and S. Galande (2015). "A comprehensive
722 epigenome map of Plasmodium falciparum reveals unique mechanisms of transcriptional regulation
723 and identifies H3K36me2 as a global mark of gene suppression." Epigenetics Chromatin **8**: 32.
724 Kim, H., L. Yen, S. P. Wongpalee, J. A. Kirshner, N. Mehta, Y. Xue, J. B. Johnston, A. L. Burlingame, J. K.
725 Kim, J. J. Loparo and S. E. Jacobsen (2019). "The Gene-Silencing Protein MORC-1 Topologically Entraps
726 DNA and Forms Multimeric Assemblies to Cause DNA Compaction." Mol Cell **75**(4): 700-710 e706.
727 Koch, A., H. G. Kang, J. Steinbrenner, D. A. Dempsey, D. F. Klessig and K. H. Kogel (2017). "MORC
728 Proteins: Novel Players in Plant and Animal Health." Front Plant Sci **8**: 1720.
729 Koyama, F. C., R. Y. Ribeiro, J. L. Garcia, M. F. Azevedo, D. Chakrabarti and C. R. Garcia (2012). "Ubiquitin
730 proteasome system and the atypical kinase PfPK7 are involved in melatonin signaling in Plasmodium
731 falciparum." J Pineal Res **53**(2): 147-153.
732 Lambros, C. and J. P. Vanderberg (1979). "Synchronization of Plasmodium falciparum erythrocytic
733 stages in culture." J Parasitol **65**(3): 418-420.
734 Le Roch, K. G., Y. Zhou, P. L. Blair, M. Grainger, J. K. Moch, J. D. Haynes, P. De La Vega, A. A. Holder, S.
735 Batalov, D. J. Carucci and E. A. Winzeler (2003). "Discovery of gene function by expression profiling of
736 the malaria parasite life cycle." Science **301**(5639): 1503-1508.
737 Lima, W. R., M. Moraes, E. Alves, M. F. Azevedo, D. O. Passos and C. R. Garcia (2013). "The PfNF-YB
738 transcription factor is a downstream target of melatonin and cAMP signalling in the human malaria
739 parasite Plasmodium falciparum." J Pineal Res **54**(2): 145-153.
740 Lima, W. R., G. Tessarin-Almeida, A. Rozanski, K. S. Parreira, M. S. Moraes, D. C. Martins, R. F.
741 Hashimoto, P. A. F. Galante and C. R. S. Garcia (2016). "Signaling transcript profile of the asexual
742 intraerythrocytic development cycle of Plasmodium falciparum induced by melatonin and cAMP."
743 Genes Cancer **7**(9-10): 323-339.
744 Love, M. I., W. Huber and S. Anders (2014). "Moderated estimation of fold change and dispersion for
745 RNA-seq data with DESeq2." Genome Biol **15**(12): 550.
746 Miao, J., C. Wang, A. B. Lucky, X. Liang, H. Min, S. R. Adapa, R. Jiang, K. Kim and L. Cui (2021). "A unique
747 GCN5 histone acetyltransferase complex controls erythrocyte invasion and virulence in the malaria
748 parasite Plasmodium falciparum." PLoS Pathog **17**(8): e1009351.
749 Modrzynska, K., C. Pfander, L. Chappell, L. Yu, C. Suarez, K. Dundas, A. R. Gomes, D. Goulding, J. C.
750 Rayner, J. Choudhary and O. Billker (2017). "A Knockout Screen of ApiAP2 Genes Reveals Networks of
751 Interacting Transcriptional Regulators Controlling the Plasmodium Life Cycle." Cell Host Microbe **21**(1):
752 11-22.
753 Moissiard, G., S. J. Cokus, J. Cary, S. Feng, A. C. Billi, H. Stroud, D. Husmann, Y. Zhan, B. R. Lajoie, R. P.
754 McCord, C. J. Hale, W. Feng, S. D. Michaels, A. R. Frand, M. Pellegrini, J. Dekker, J. K. Kim and S. E.
755 Jacobsen (2012). "MORC family ATPases required for heterochromatin condensation and gene
756 silencing." Science **336**(6087): 1448-1451.
757 Painter, H. J., T. L. Campbell and M. Llinas (2011). "The Apicomplexan AP2 family: integral factors
758 regulating Plasmodium development." Mol Biochem Parasitol **176**(1): 1-7.
759 Patro, R., G. Duggal, M. I. Love, R. A. Irizarry and C. Kingsford (2017). "Salmon provides fast and bias-
760 aware quantification of transcript expression." Nat Methods **14**(4): 417-419.
761 Perez-Riverol, Y., J. Bai, C. Bandla, D. Garcia-Seisdedos, S. Hewapathirana, S. Kamatchinathan, D. J.
762 Kundu, A. Prakash, A. Frericks-Zipper, M. Eisenacher, M. Walzer, S. Wang, A. Brazma and J. A. Vizcaino
763 (2022). "The PRIDE database resources in 2022: a hub for mass spectrometry-based proteomics
764 evidences." Nucleic Acids Res **50**(D1): D543-D552.
765 Pradhan, A., V. S. Chauhan and R. Tuteja (2005). "Plasmodium falciparum DNA helicase 60 is a schizont
766 stage specific, bipolar and dual helicase stimulated by PKC phosphorylation." Mol Biochem Parasitol
767 **144**(2): 133-141.
768 Quinn, J. E., M. D. Jeninga, K. Limm, K. Pareek, T. Meissgeier, A. Bachmann, M. F. Duffy and M. Petter
769 (2022). "The Putative Bromodomain Protein PfBDP7 of the Human Malaria Parasite Plasmodium
770 Falciparum Cooperates With PfBDP1 in the Silencing of Variant Surface Antigen Expression." Front Cell
771 Dev Biol **10**: 816558.

Russell, T. J., E. K. De Silva, V. M. Crowley, K. Shaw-Saliba, N. Dube, G. Josling, C. F. A. Pasaje, I. Kouskoumvekaki, G. Panagiotou, J. C. Niles, M. Jacobs-Lorena, C. Denise Okafor, F. J. Gamo and M. Llinas (2022). "Inhibitors of ApiAP2 protein DNA binding exhibit multistage activity against Plasmodium parasites." PLoS Pathog **18**(10): e1010887.

Santos, J. M., G. Josling, P. Ross, P. Joshi, L. Orchard, T. Campbell, A. Schieler, I. M. Cristea and M. Llinas (2017). "Red Blood Cell Invasion by the Malaria Parasite Is Coordinated by the PfAP2-I Transcription Factor." Cell Host Microbe **21**(6): 731-741 e710.

Sargeant, T. J., M. Marti, E. Caler, J. M. Carlton, K. Simpson, T. P. Speed and A. F. Cowman (2006). "Lineage-specific expansion of proteins exported to erythrocytes in malaria parasites." Genome Biol **7**(2): R12.

Scherf, A., R. Hernandez-Rivas, P. Buffet, E. Bottius, C. Benatar, B. Pouvelle, J. Gysin and M. Lanzer (1998). "Antigenic variation in malaria: in situ switching, relaxed and mutually exclusive transcription of var genes during intra-erythrocytic development in Plasmodium falciparum." EMBO J **17**(18): 5418-5426.

Scherf, A., J. J. Lopez-Rubio and L. Riviere (2008). "Antigenic variation in Plasmodium falciparum." Annu Rev Microbiol **62**: 445-470.

Schuck, D. C., A. K. Jordao, M. Nakabashi, A. C. Cunha, V. F. Ferreira and C. R. Garcia (2014). "Synthetic indole and melatonin derivatives exhibit antimalarial activity on the cell cycle of the human malaria parasite Plasmodium falciparum." Eur J Med Chem **78**: 375-382.

Shang, X., S. Shen, J. Tang, X. He, Y. Zhao, C. Wang, X. He, G. Guo, M. Liu, L. Wang, Q. Zhu, G. Yang, C. Jiang, M. Zhang, X. Yu, J. Han, R. Culleton, L. Jiang, J. Cao, L. Gu and Q. Zhang (2021). "A cascade of transcriptional repression determines sexual commitment and development in Plasmodium falciparum." Nucleic Acids Res **49**(16): 9264-9279.

Shang, X., C. Wang, Y. Fan, G. Guo, F. Wang, Y. Zhao, F. Sheng, J. Tang, X. He, X. Yu, M. Zhang, G. Zhu, S. Yin, J. Mu, R. Culleton, J. Cao, M. Jiang and Q. Zhang (2022). "Genome-wide landscape of ApiAP2 transcription factors reveals a heterochromatin-associated regulatory network during Plasmodium falciparum blood-stage development." Nucleic Acids Res **50**(6): 3413-3431.

Shang, X., C. Wang, L. Shen, F. Sheng, X. He, F. Wang, Y. Fan, X. He and M. Jiang (2021). "PfAP2-EXP2, an Essential Transcription Factor for the Intraerythrocytic Development of Plasmodium falciparum." Front Cell Dev Biol **9**: 782293.

Sierra-Miranda, M., S. S. Vembar, D. M. Delgadillo, P. A. Avila-Lopez, A. M. Herrera-Solorio, D. Lozano Amado, M. Vargas and R. Hernandez-Rivas (2017). "PfAP2Tel, harbouring a non-canonical DNA-binding AP2 domain, binds to Plasmodium falciparum telomeres." Cell Microbiol **19**(9).

Singh, M. K., G. Tessarin-Almeida, B. K. M. Dias, P. S. Pereira, F. Costa, J. M. Przyborski and C. R. S. Garcia (2021). "A nuclear protein, PfMORC confers melatonin dependent synchrony of the human malaria parasite P. falciparum in the asexual stage." Sci Rep **11**(1): 2057.

Singh, S., M. M. Alam, I. Pal-Bhowmick, J. A. Brzostowski and C. E. Chitnis (2010). "Distinct external signals trigger sequential release of apical organelles during erythrocyte invasion by malaria parasites." PLoS Pathog **6**(2): e1000746.

Singh, S., J. M. Santos, L. M. Orchard, N. Yamada, R. van Biljon, H. J. Painter, S. Mahony and M. Llinas (2021). "The PfAP2-G2 transcription factor is a critical regulator of gametocyte maturation." Mol Microbiol **115**(5): 1005-1024.

Sinha, A., K. R. Hughes, K. K. Modrzynska, T. D. Otto, C. Pfander, N. J. Dickens, A. A. Religa, E. Bushell, A. L. Graham, R. Cameron, B. F. C. Kafsack, A. E. Williams, M. Llinas, M. Berriman, O. Billker and A. P. Waters (2014). "A cascade of DNA-binding proteins for sexual commitment and development in Plasmodium." Nature **507**(7491): 253-257.

Smith, L. M., F. C. Motta, G. Chopra, J. K. Moch, R. R. Nerem, B. Cummins, K. E. Roche, C. M. Kelliher, A. R. Leman, J. Harer, T. Gedeon, N. C. Waters and S. B. Haase (2020). "An intrinsic oscillator drives the blood stage cycle of the malaria parasite Plasmodium falciparum." Science **368**(6492): 754-759.

Soneson, C., M. I. Love and M. D. Robinson (2015). "Differential analyses for RNA-seq: transcript-level estimates improve gene-level inferences." F1000Res **4**: 1521.

Srinivasan, P., A. Yasgar, D. K. Luci, W. L. Beatty, X. Hu, J. Andersen, D. L. Narum, J. K. Moch, H. Sun, J. D. Haynes, D. J. Maloney, A. Jadhav, A. Simeonov and L. H. Miller (2013). "Disrupting malaria parasite AMA1-RON2 interaction with a small molecule prevents erythrocyte invasion." Nat Commun **4**: 2261.

Srivastava, S., M. J. Holmes, M. W. White and W. J. Sullivan, Jr. (2023). "Toxoplasma gondii AP2XII-2 Contributes to Transcriptional Repression for Sexual Commitment." mSphere **8**(2): e0060622.

Strahl, B. D., P. A. Grant, S. D. Briggs, Z. W. Sun, J. R. Bone, J. A. Caldwell, S. Mollah, R. G. Cook, J. Shabanowitz, D. F. Hunt and C. D. Allis (2002). "Set2 is a nucleosomal histone H3-selective methyltransferase that mediates transcriptional repression." Mol Cell Biol **22**(5): 1298-1306.

Subudhi, A. K., J. L. Green, R. Satyam, T. Lenz, R. P. Salunke, M. Shuaib, I. Isaioglou, S. Abel, M. Gupta, L. Esau, T. Mourier, R. Nugmanova, S. Mfarrej, R. Sivapurkar, Z. Stead, F. B. Rached, Y. Otswal, R. Sougrat, A. Dada, A. F. Kadamany, W. Fischle, J. Merzaban, E. Knuepfer, D. J. P. Ferguson, I. Gupta, K. G. L. Roch, A. A. Holder and A. Pain (2023). "PfAP2-MRP DNA-binding protein is a master regulator of parasite pathogenesis during malaria parasite blood stages." bioRxiv: 2023.2005.2023.541898.

Subudhi, A. K., A. J. O'Donnell, A. Ramaprasad, H. M. Abkallo, A. Kaushik, H. R. Ansari, A. M. Abdel-Haleem, F. Ben Rached, O. Kaneko, R. Culleton, S. E. Reece and A. Pain (2020). "Malaria parasites regulate intra-erythrocytic development duration via serpentine receptor 10 to coordinate with host rhythms." Nat Commun **11**(1): 2763.

Toenhake, C. G., S. A. Fraschka, M. S. Vijayabaskar, D. R. Westhead, S. J. van Heeringen and R. Bartfai (2018). "Chromatin Accessibility-Based Characterization of the Gene Regulatory Network Underlying Plasmodium falciparum Blood-Stage Development." Cell Host Microbe **23**(4): 557-569 e559.

Trager, W. and J. B. Jensen (1976). "Human malaria parasites in continuous culture." Science **193**(4254): 673-675.

Wagner, E. J. and P. B. Carpenter (2012). "Understanding the language of Lys36 methylation at histone H3." Nat Rev Mol Cell Biol **13**(2): 115-126.

Ward, P., L. Equinet, J. Packer and C. Doerig (2004). "Protein kinases of the human malaria parasite Plasmodium falciparum: the kinome of a divergent eukaryote." BMC Genomics **5**: 79.

Yeoh, S., R. A. O'Donnell, K. Koussis, A. R. Dluzewski, K. H. Ansell, S. A. Osborne, F. Hackett, C. Withers-Martinez, G. H. Mitchell, L. H. Bannister, J. S. Bryans, C. A. Kettleborough and M. J. Blackman (2007). "Subcellular discharge of a serine protease mediates release of invasive malaria parasites from host erythrocytes." Cell **131**(6): 1072-1083.

Yuda, M., S. Iwanaga, S. Shigenobu, G. R. Mair, C. J. Janse, A. P. Waters, T. Kato and I. Kaneko (2009). "Identification of a transcription factor in the mosquito-invasive stage of malaria parasites." Mol Microbiol **71**(6): 1402-1414.

Yuda, M., I. Kaneko, Y. Murata, S. Iwanaga and T. Nishi (2023). "Targetome Analysis of Malaria Sporozoite Transcription Factor AP2-Sp Reveals Its Role as a Master Regulator." mBio **14**(1): e0251622.

Zhang, M., C. Wang, T. D. Otto, J. Oberstaller, X. Liao, S. R. Adapa, K. Udenze, I. F. Bronner, D. Casandra, M. Mayho, J. Brown, S. Li, J. Swanson, J. C. Rayner, R. H. Y. Jiang and J. H. Adams (2018). "Uncovering the essential genes of the human malaria parasite Plasmodium falciparum by saturation mutagenesis." Science **360**(6388).

Zhang, Y., B. Bertulat, A. H. Tencer, X. Ren, G. M. Wright, J. Black, M. C. Cardoso and T. G. Kutateladze (2019). "MORC3 Forms Nuclear Condensates through Phase Separation." iScience **17**: 182-189.

Zhong, Z., Y. Xue, C. J. Harris, M. Wang, Z. Li, Y. Ke, M. Liu, J. Zhou, Y. Jami-Alahmadi, S. Feng, J. A. Wohlschlegel and S. E. Jacobsen (2023). "MORC proteins regulate transcription factor binding by mediating chromatin compaction in active chromatin regions." Genome Biol **24**(1): 96.

869 **Figures –**

870

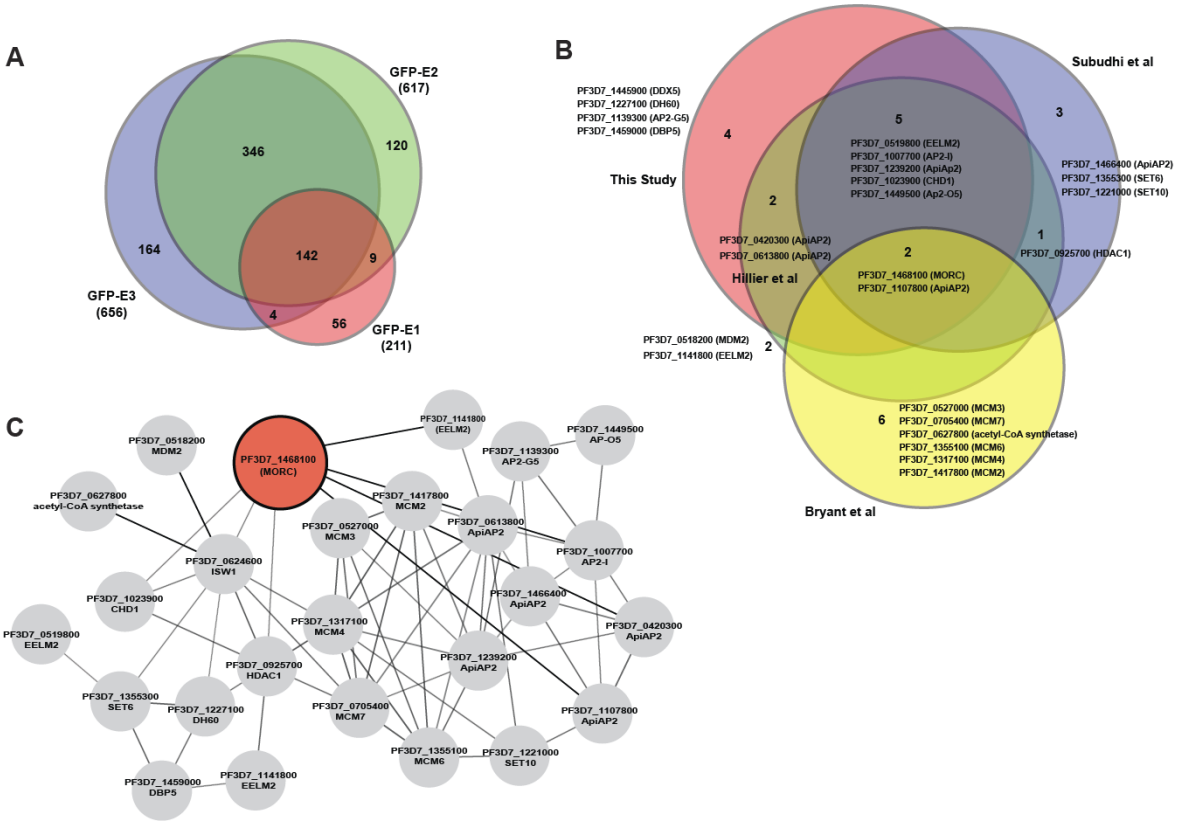

871

872 **Figure 1 – Proteomic analysis of parasites expressing *Pf*MORC^{GFP} reveals *Pf*MORC**
873 **association with nuclear proteins of epigenetic regulation. (A)** Venn diagram depicting
874 protein enrichment from three biological replicates using *Pf*MORC as bait from 32 hpi (±4 h)
875 trophozoite stage *Pf*MORC^{GFP} parasite lysate with anti-GFP-Trap-A beads. **(B)** Venn diagram
876 was created for CoIPed protein in PfMORC^{GFP} with selected proteins from recently published
877 work by Hillier et al, Bryant et al. and Subudhi et al. Intersecting proteins showing the majority
878 of proteins are AP2 and chromatin remodellers. **(C)** Protein-protein interaction network of
879 enriched proteins co-IPed with anti-GFP and detected by mass spectrometry was generated with
880 known *Pf*MORC interactome from published work. The String database and Cytoscape were
881 used to create an interactive protein-protein interaction network.

882

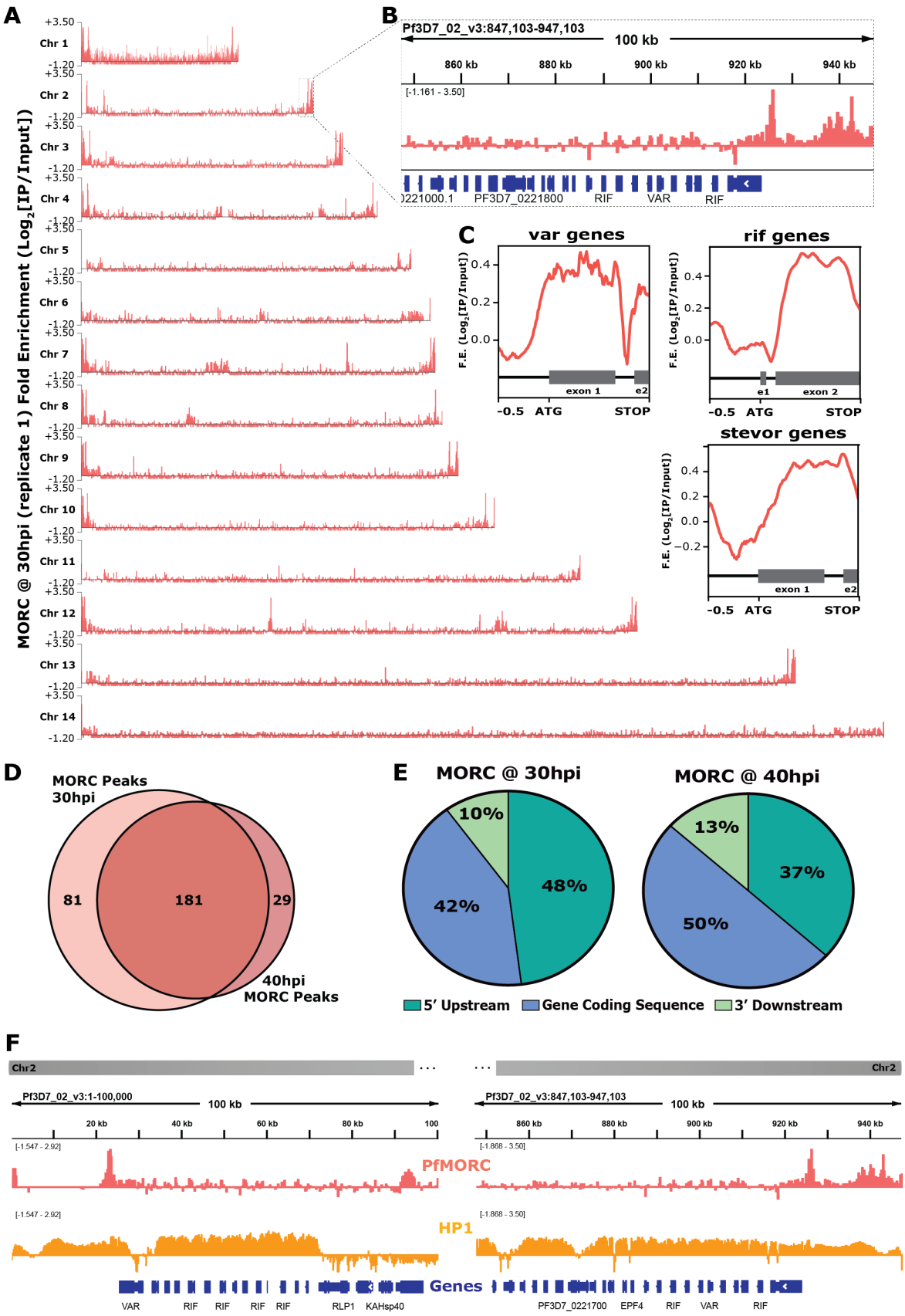

Figure 2 – Genome-wide occupancy of PfMORC reveals localization to hypervariable surface antigen genes at 30 h and 40 h. (A) Coverage tracks of PfMORC across all 14 *P. falciparum* chromosomes. Plotted values are fold enrichment (Log2[IP/Input]) of a

representative replicate at 30 h. **(B)** Zoom-in of the last 100kb region of chromosome two from Panel A. Gene annotations represented in blue bars (*P. falciparum* 3D7 strain, version 3, release 57; PlasmoDB.org). **(C)** Mean fold enrichment of PfMORC occupancy across all var genes (top left), all rif genes (top right), and all stevor genes (bottom right), excluding pseudogenes. Graphical representation of exons to scale for each gene family annotated below enrichment plot in grey (e1=exon one; e2=exon two). **(D)** Quantitative Venn diagram comparing the number of MACS2 called peaks across each timepoint (light pink for 30 h; dark pink for 40 h). **(E)** Pie charts showing the type of genomic locations PfMORC peaks overlap at both 30 h and 40 h. Pink slices are 5` regions upstream of the ATG start site of genes, blue slices are coding sequences/gene bodies of genes, and green slices are 3` regions downstream of the stop codon of genes. **(F)** Zoom-in of the first 100kb region (left) and the last 100kb region (right) of chromosome two. Plotted are the ChIP-seq fold enrichment of PfMORC (top track; pink) and heterochromatin protein 1 (HP1; middle track; orange) with gene annotations (bottom track; blue bars; *P. falciparum* 3D7 strain, version 3, release 57; PlasmoDB.org).

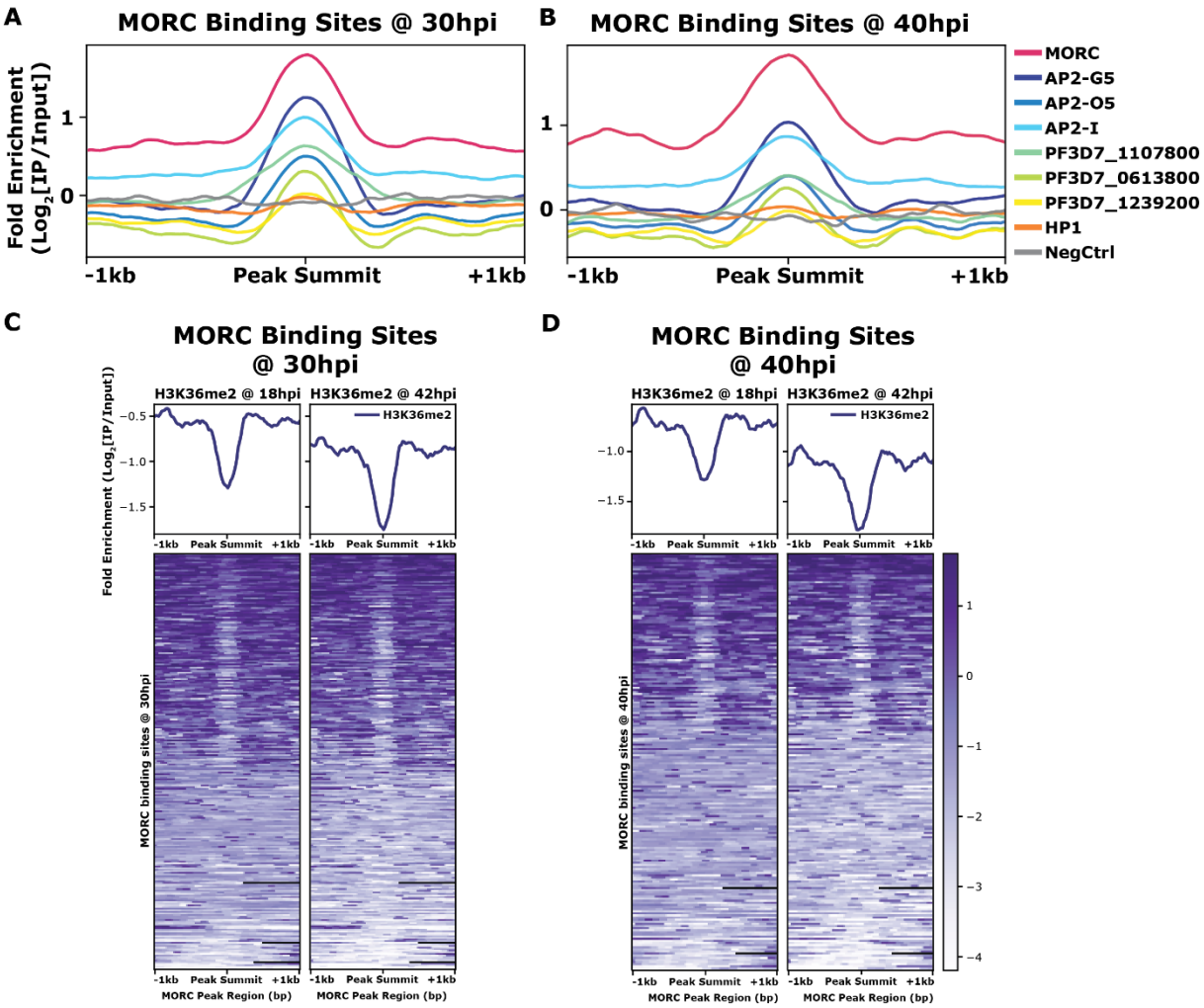

Figure 3 – **(A)** Mean fold enrichment (Log2[IP/Input]) of PfMORC, six associated factors (AP2-G5, AP2-O5, AP2-I, PF3D7_1107800, PF3D7_0613800, and PF3D7_1239200), HP1, and a negative no-epitope control across PfMORC binding sites at the 30 h timepoint. **(B)** Mean fold enrichment (Log2[IP/Input]) of PfMORC, six associated factors (AP2-G5, AP2-O5, AP2-I, PF3D7_1107800, PF3D7_0613800, and PF3D7_1239200), HP1, and a negative no-epitope control across PfMORC binding sites at the 40 h timepoint. **(C)** Mean fold enrichment (Log2[IP/Input]) and heatmap of two H3K36me2 epigenetic mark timepoints across PfMORC binding sites at 30 h. **(D)** Mean fold enrichment (Log2[IP/Input]) and heatmap of two H3K36me2 epigenetic mark timepoints across PfMORC binding sites at 40 h.

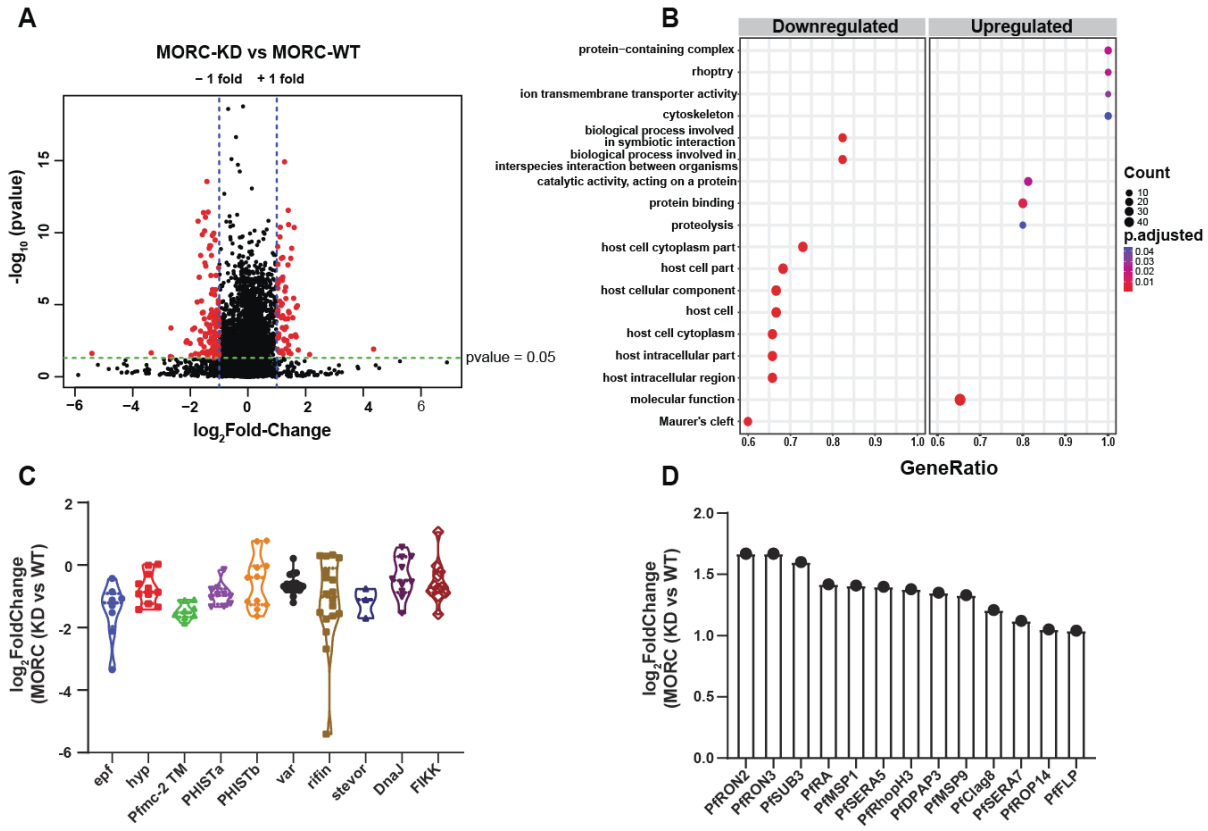

Figure 4 – Transcriptome analysis of *Pf*MORC knockdown revealed differential gene expression. (**A**) Volcano plot showing the differential gene expression in *Pf*MORC-KD compared to the *Pf*MORC-WT phenotype. Tightly synchronized parasites were treated with 2.5 mM GlcN to obtain the *Pf*MORC knockdown phenotype and another without GlcN treatment. Total RNA was collected from three biological replicates, and RNA-seq was performed. Significant threshold parameters for DEGs were assigned to a p value < 0.05. **(B)** Up and downregulated DEGs were further functionally categorized using KEGG database. **(C)** The violin plot of log_2FoldChange of genes belonging to the multigene family is constructed from *Pf*MORC-KD vs *Pf*MORC-WT shows DEGs of multigene family proteins upon *Pf*MORC knockdown. **(D)** The bar plot shows upregulated DEGs of apical organelle origin in *Pf*MORC-KD parasites that are involved in host cell invasion. **(E)** Venn diagram showing the comparison between genes obtained from ChIP-seq data and DEGs obtained from RNA-seq data. Both 30hpi and 40 hpi time points were taken for comparison and showed high overlap with each other but there was no overlap with RNA-seq data.

939 **Supplemental Figures**

940

941 **Supplemental Figure 1 –**

942 **(A)** Coomassie-stained 6% SDS–PAGE gel showing the parasite lysate of wild-type 3D7 and
943 *Pf*MORC^{GFP} after coimmunoprecipitation with anti-GFP magnetic beads. Both lanes were used
944 for mass spectrometry analysis. **(B)** Histogram shows the total proteins identified in mass
945 spectrometry analysis from three biological replicates in wild-type 3D7 and *Pf*MORC^{GFP}
946 coimmunoprecipitated samples. **(C)** Venn diagram showing protein enrichment in 3D7 control
947 samples from three biological replicates from 32 hpi (±4 h) trophozoite stage with anti-GFP-
948 Trap-A beads which is used for normalization. **(D)** MS/MS normalization of identified proteins
949 from 3D7 parasites expressing *Pf*MORC and transgenic parasites expressing GFP
950 (*Pf*MORC^{GFP}) was carried out. Gene ontology classification showing biological process,
951 cellular component, and molecular function of *Pf*MORC^{GFP}/3D7 normalized proteins showing
952 fold change ≥ 1.5.

953

954 **Supplemental Figure 2 –**

955 **(A)** Correlation plot (DeepTools PlotCorrelation) of the 30 h samples compared to the negative
956 control ChIP-seq sample. **(B)** Correlation plot (DeepTools PlotCorrelation) of the 40 h samples
957 compared to the negative control ChIP-seq sample. **(C)** Violin plot showing the ChIP-seq fold
958 enrichment values of significantly called peaks in all 6 biological replicates. The two GFP
959 samples were only used as additional controls for comparison purposes. **(D)** Venn diagram
960 comparing the overlap of MACS2-called peaks between anti-HA biological replicates at 30 h.
961 **(E)** Venn diagram comparing the overlap of MACS2-called peaks between anti-HA biological
962 replicates at 40 h. (F) Venn diagram comparing the overlap of MACS2-called peaks between
963 anti-GFP biological replicates at 40 h.

964

965 **Supplemental Figure 3 –**

966 **(Top)** Profile plot of the mean PfMORC ChIP-seq fold enrichment (Log2[IP/Input]) for all four
967 samples across all PfEMP1 (var) gene 5` upstream regions and gene bodies. **(Bottom)** Heatmap
968 of the PfMORC ChIP-seq fold enrichment (Log2[IP/Input]) for all four samples across all
969 PfEMP1 (*var*) gene 5` upstream regions and gene bodies. **(Inset to the right)** Zoom in on the
970 average enrichment of PfMORC at var genes with annotated exons.

971

972 **Supplemental Figure 4 –**

973 **(Top)** Profile plot of the mean PfMORC ChIP-seq fold enrichment (Log2[IP/Input]) for all four
974 samples across all *rif* gene 5` upstream regions and gene bodies. **(Bottom)** Heatmap of the
975 PfMORC ChIP-seq fold enrichment (Log2[IP/Input]) for all four samples across all *rif* gene 5`
976 upstream regions and gene bodies. **(Inset to the right)** Zoom in on the average enrichment of
977 PfMORC at *rif* genes with annotated exons.

978

979

980 **Supplemental Figure 5 –**

981 **(Top)** Profile plot of the mean PfMORC ChIP-seq fold enrichment (Log2[IP/Input]) for all four
982 samples across all *rif* gene 5` upstream regions and gene bodies. **(Bottom)** Heatmap of the
983 PfMORC ChIP-seq fold enrichment (Log2[IP/Input]) for all four samples across all *rif* gene 5`
984 upstream regions and gene bodies. **(Inset to the right)** Zoom in on the average enrichment of
985 PfMORC at *rif* genes with annotated exons.

986

987 **Supplemental Figure 6 –**

988 The heatmaps show the transcript abundance (Chappell et al. 2020) of putative PfMORC gene
989 targets at 30 h (left) and 40 h (right). Red signifies high transcript abundance, and green signifies
990 low transcript abundance. Both timepoints are organized into two major clusters (highlighted
991 with the yellow bar and blue bar).

992

993 **Supplemental Figure 7 –**

994 **(A)** Associated with Figure 3A,B. Mean fold enrichment (Log2[IP/Input]) summary plot (top) and
995 full heatmap (bottom) of fold enrichment of PfMORC, six associated ApiAP2 factors (AP2-
996 G5, AP2-O5, AP2-I, PF3D7_1107800, PF3D7_0613800, and PF3D7_1239200), HP1, and a
997 negative no-epitope control across PfMORC binding sites at the 30 h and 40 h timepoints. **(B)**
998 Quantitative Venn diagrams of the binding site overlaps between PfMORC and the six associated
999 ApiAP2 factors.

1000

1001 **Supplemental Figure 8 –**

1002 DNA motif analyses from these different categories: (1) Unique to 30 hpi ChIP-seq Timepoint,
1003 (2) 30hpi ChIP-seq Timepoint, (3) Overlap of ChIP-seq Timepoints, (4) 40hpi ChIP-seq
1004 Timepoint, and (5) Unique to 30hpi ChIP-seq Timepoint. The values to the right of each motif
1005 contain the enrichment value, number of peaks containing that motif, and percent of the peaks
1006 the contain that motif calculated by Meme Suite.

1007

1008 **Supplemental Figure 9 –**

1009 Mean fold enrichment (Log2[IP/Input]) summary plot (top) and full heatmap (bottom) of fold
1010 enrichment of ten selected epigenetic marks (H2A.Z, H3K9ac, H3K4me3, H3K27ac, H3K18ac,
1011 H3K9me3, H3K36me2/3, H4K20me3, and H3K4me1) across PfMORC binding sites at the 30
1012 h and 40 h timepoints.

1013

1014 **Supplemental Figure 10 –**

1015 **Comparison of transcriptional changes with melatonin treatment. (A)** Volcano plot
1016 showing the differentially expressed genes in *Pf*MORC-KD parasites relative to *Pf*MORC-WT
1017 after 100 nM melatonin treatment. **(B)** Venn diagram shows intersecting DEGs from the
1018 experiment with KD vs WT with DEGs obtained from the experiment (KD vs WT) treated with
1019 100 nM melatonin for 5 h. Number of DEGs are shown as up (red) and downregulated (green).
1020 The intersecting region shows 282 upregulated and 340 downregulated genes. Heatmap

1021 showing significant DEGs based on p values and log_2FD for upregulating (**C**) and
1022 downregulating (**D**). These genes are taken from 622 intersecting DEGs showing partial
1023 changes in expression after melatonin treatment.

1024